iScience

CellPress
OPEN ACCESS

Article

Intracellular C4BPA Levels Regulate NF-κB-Dependent Apoptosis

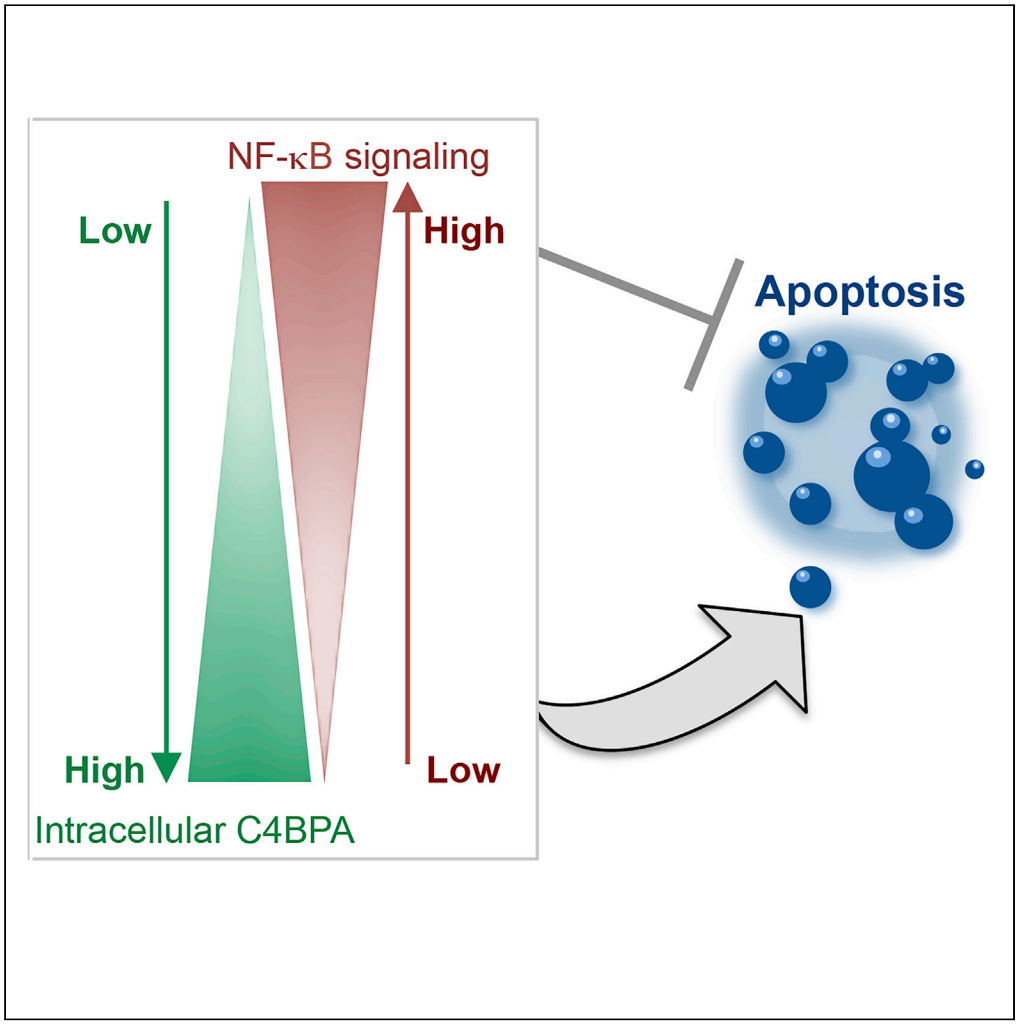

Monica M. Olcina, Ryan K. Kim, Nikolas G. Balanis, ..., Daniel Ricklin, Manuel Stucki, Amato J. Giaccia

monica.olcinadelmolino@uzh.ch

HIGHLIGHTS

C4BPA mutations are associated with improved overall survival in 23 tumor types

C4BPA is found, for the first time, to interact with NF-κB family member RelA

C4BPA expression is regulated in a mutation- and stress-responsive manner

C4BPA has a non-canonical intracellular function in regulating NF-κB signaling

Olcina et al., iScience *23*, 101594
October 23, 2020
https://doi.org/10.1016/j.isci.2020.101594

iScience

CellPress
OPEN ACCESS

Article

Intracellular C4BPA Levels Regulate NF-κB-Dependent Apoptosis

Monica M. Olcina,[1,5,7,*] Ryan K. Kim,[1] Nikolas G. Balanis,[2] Caiyun Grace Li,[1] Rie von Eyben,[1] Thomas G. Graeber,[3] Daniel Ricklin,[4] Manuel Stucki,[5] and Amato J. Giaccia[1,6]

SUMMARY

The importance of innate immunity in cancer is increasingly being recognized with recent reports suggesting tumor cell-intrinsic intracellular functions for innate immunity proteins. However, such functions are often poorly understood, and it is unclear whether these are affected by patient-specific mutations. Here, we show that C4b-binding protein alpha chain (C4BPA), typically thought to reside in the extracellular space, is expressed intracellularly in cancer cells, where it interacts with the NF-κB family member RelA and regulates apoptosis. Interestingly, intracellular C4BPA expression is regulated in a stress- and mutation-dependent manner and *C4BPA* mutations are associated with improved cancer survival outcome. Using cell lines harboring patient-specific *C4BPA* mutations, we show that increasing intracellular C4BPA levels correlate with sensitivity to oxaliplatin-induced apoptosis *in vitro* and *in vivo*. Mechanistically, sensitive *C4BPA* mutants display increased IκBα expression and increased inhibitory IκBα-RelA complex stability. These data suggest a non-canonical intracellular role for C4BPA in regulating NF-κB-dependent apoptosis.

INTRODUCTION

The importance of innate immunity in cancer is increasingly being recognized, with innate immune pathways involved in inflammation, cytosolic nucleic acid sensing, and adaptive immune activation (Hoesel and Schmid, 2013; MacKenzie et al., 2017). NF-κB family members often regulate downstream effector functions (such as inflammation and apoptosis) of innate immunity players (Dunphy et al., 2018; Legrand et al., 2019). NF-κB-dependent transactivation occurs through either the canonical or non-canonical pathways (Karin and Lin, 2002; Hoesel and Schmid, 2013). The canonical NF-κB pathway refers to heterodimers of RelA, c-Rel, and p50, which under unstimulated conditions are retained in the cytoplasm through interaction with inhibitors such as the IκB proteins (IκBα, IκBβ, IκBε or p105 and IκBγ) (Karin and Lin, 2002). In response to stimuli such as cytotoxic therapy, activation of the IκB kinase (IKK) complex (including IKKα, IKKβ, and IKKγ) leads to IKK-dependent phosphorylation of IκBα, targeting it for proteasomal degradation. IκBα degradation allows translocation of NF-κB dimers (the most abundant being p50-RelA) to the nucleus and activation of NF-κB target genes including anti-apoptotic targets (Barkett and Gilmore, 1999; Chen et al., 2000; Karin and Lin, 2002).

In the non-canonical pathway, activation of NF-κB occurs following binding of 'non-canonical pathway ligands' such as CD40L. Ligand binding allows phosphorylation of IKKα by NF-κB-inducing kinase (NIK). IKKα phosphorylates precursor protein p100 (IκBδ) triggering ubiquitination and partial proteasomal degradation to p52. p52 can then form a DNA-binding heterodimer with RelB, which translocates to the nucleus to induce a transcriptional program. NF-κB inhibition in cancer cells reduces NF-κB-dependent activation of anti-apoptotic genes and is well known to increase sensitivity of cell lines to cytotoxic chemotherapy and radiotherapy (Barkett and Gilmore, 1999; Chen et al., 2000; Karin and Lin, 2002).

A comprehensive understanding of how cooperation between innate immunity pathways is modulated in response to cytotoxic therapies will yield important insights relevant for our understanding of how to improve cancer therapies. Importantly, we recently reported that somatic mutations in a key innate immunity pathway, the complement system, are widespread across cancer types and correlate with overall survival outcome, suggesting they might modulate responses to standard-of-care agents (Olcina et al., 2018). The complement system

[1]Department of Radiation Oncology, Stanford University, Stanford, CA 94305, USA

[2]Department of Molecular and Medical Pharmacology, Crump Institute for Molecular Imaging, David Geffen School of Medicine, University of California, Los Angeles, CA, USA

[3]Department of Molecular and Medical Pharmacology, Crump Institute for Molecular Imaging, Jonsson Comprehensive Cancer Center, David Geffen School of Medicine, University of California, Los Angeles, CA, USA

[4]Department of Pharmaceutical Sciences, University of Basel, Klingelbergstrasse 50, 4056 Basel, Switzerland

[5]Department of Gynecology, University of Zurich, Wagistrasse 14, 8952 Schlieren, Switzerland

[6]Oxford Institute of Radiation Oncology, University of Oxford, Old Road Campus Research Building, Roosevelt Drive, Oxford OX37DQ, UK

[7]Lead Contact

*Correspondence: monica.olcinadelmolino@uzh.ch

https://doi.org/10.1016/j.isci.2020.101594

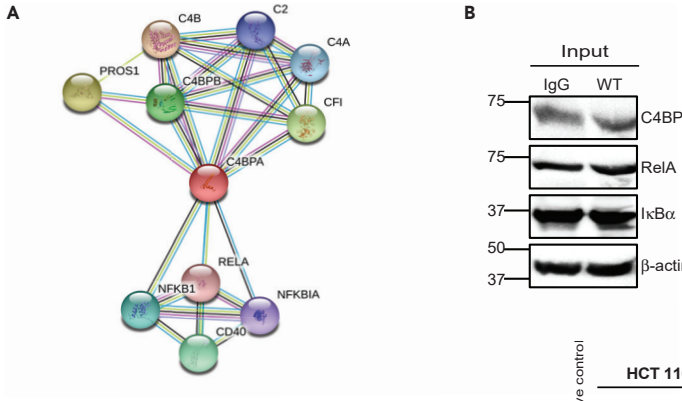

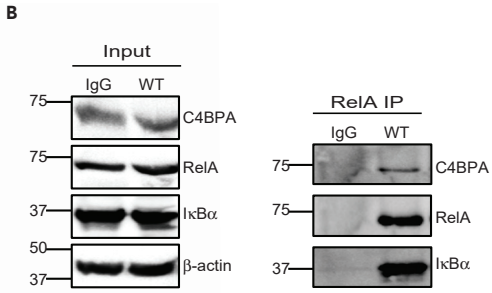

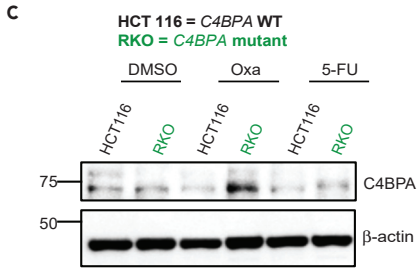

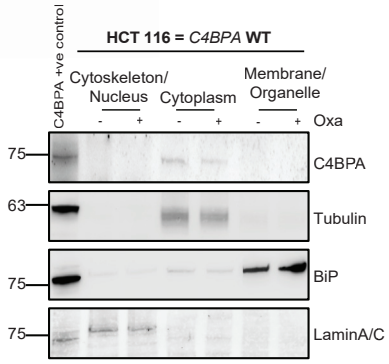

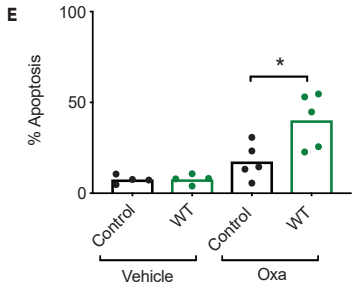

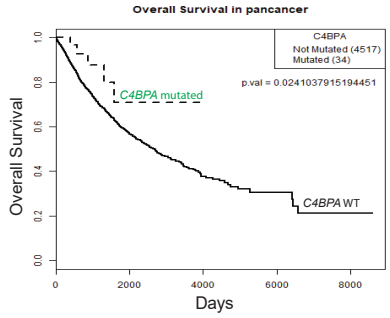

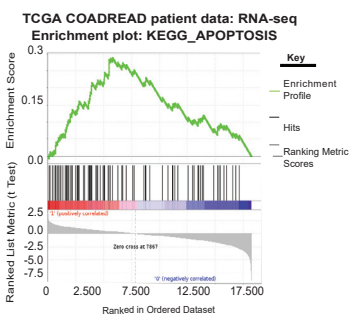

H

TCGA COADREAD patient data: RPPA

Term	P-Value	FDR
Regulation of apoptosis	3.73E-08	5.70E-05
Regulation of programmed cell death	4.13E-08	6.31E-05
Regulation of cell death	4.29E-08	6.56E-05

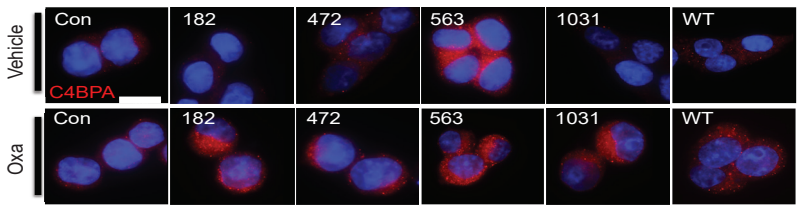

Figure 1. Intracellular C4BPA Interacts with RelA

(A) String.org protein-protein interaction network for C4BPA. Light blue line = known interaction from curated database, pink line = known interaction experimentally tested, dark green line = predicted interaction, gene neighborhood, light green line = text mining interaction source, black line = co-expression interaction source, light purple line = protein homology interaction source.

(B) HCT 116 *C4BPA*^{WT} cells were transfected with either wild-type (WT) *C4BPA* or pcDNA3.1. Pull-down with RelA antibody was performed, and input and immunoprecipitation (IP) for the pull-down is shown. Input was collected from the same experiment as the pull-down shown. Western blotting was carried out with the antibodies indicated. n = 2. IgG control is shown in the left lane of the blot.

(C) RKO (colorectal cancer cells with endogenous *C4BPA* mutation) and HCT 116 (colorectal cancer cells without *C4BPA* mutation) were treated with DMSO, oxaliplatin (40 μM, 24 h), or 5-FU (0.1 μg/mL, 24 h). Western blotting was carried out with the antibodies indicated. β-Actin was used as the loading control. n = 3.

(D) Cellular fractionation followed by western blotting was carried out in HCT 116 *C4BPA*^{WT} treated with oxaliplatin (40 μM, 24 h). Tubulin was used as a control for the cytoplasm fraction, and LaminA/C was used as a nuclear fraction control. Lysate from cells transfected with WT *C4BPA* was loaded on the right hand side of the gel as a positive control for the detection of intracellular C4BPA, n = 2.

(E) HCT 116 cells where C4BPA had been depleted by CRISPR/Cas9 technology were transfected with a *C4BPA* WT construct (labeled WT OE). The parental line is also shown for comparison (labeled control). Cells were treated with oxaliplatin (40 μM, 24 h). The graph represents the number of apoptotic/non-apoptotic cells expressed as a % of the whole population. Individual dots represent values for each independent experiment. Statistical significance was evaluated by unpaired t test, * = $p < 0.05$.

(F) KM curve for overall survival of patients with mutations in *C4BPA* vs patients without mutation across pan-cancer TCGA data sets ($p = 0.0241$).

(G) GSEA plot for KEGG pathway 'Apoptosis' which appears significantly enriched in patients with mutations in *C4BPA* compared to no mutation in this gene in COADREAD patients when RNA-seq data are compared. p value = 0.001605, q value = 0.0598. NES = 2.48927.

(H) Table showing top enriched pathways in COADREAD patients with *C4BPA* mutations (compared to patients without *C4BPA* mutations) when proteins shown to be differentially expressed in RPPA data are compared and analyzed through DAVID bioinformatics resource.

(I) HCT 116 cells where C4BPA had been depleted by CRISPR-Cas9 technology were transfected with *C4BPA*-mutant constructs, each representing a mutation found in colorectal cancer TCGA patients or WT *C4BPA*. The parental line is also shown for comparison (labeled con). Cells were treated with oxaliplatin (40 μM, 24 h) and stained for C4BPA. Representative images are shown. C4BPA = red. DAPI = blue. Scale bar (shown as white bar) = 10.9 μm.

See also Figure S1.

is composed of over 40 family members, most of which are thought to be soluble or cell surface proteins having innate immune functions (Sayegh et al., 2014; Ricklin et al., 2016; Reis et al., 2017). As a first line-of-defense system, complement is well poised to exert innate immune effector functions and coordinate with defense pathways in order to mount an appropriate response to invading or foreign species (Ricklin et al., 2016). Although complement is increasingly recognized as a contributor to tumor progression and treatment responses, many aspects of its role in cancer remain to be explored (Reis et al., 2017). The presence of widespread mutations in cancer cells suggests that complement-related genes might exert effects inside tumor cells that may be distinct from their canonical functions. A deeper insight into such intracellular functions, and how they may regulate the interplay with other innate immunity pathways, will be important to further our understanding of tumor progression and treatment response. Here, we show that C4b-binding protein alpha chain (C4BPA), usually uniquely thought to form part of extracellular complement regulator C4b-binding protein (C4BP), is expressed intracellularly in colorectal cancer cells. Furthermore, we report that, intracellularly, C4BPA interacts with NF-κB pathway member RelA and that increased C4BPA levels regulate NF-κB-mediated anti-apoptotic responses following oxaliplatin treatment.

RESULTS

C4BPA Interacts with RelA

In an attempt to identify previously uncharacterized functions for negative complement regulators, we searched the STRING database for their predicted functional partners (string-db.org). We noted that C4BPA, forming part of complement regulator C4BP, had non-complement associated predicted partners. Specifically, three members of the NF-κB pathway (RelA, NF-κB1 and NF-κB inhibitor, IκBα), were predicted to be present in close interaction nodes with C4BPA (Figure 1A). Intrigued by this prediction, we performed immunoprecipitation (IP) experiments to validate the interaction between C4BPA and NF-κB family members. Since we had previously shown that negative complement regulators are expressed in colorectal cancer cell lines, we chose to perform IP experiments in HCT 116 colorectal cancer cells (Olcina et al., 2018).

IP experiments demonstrated that intracellular C4BPA interacts with NF-κB pathway member RelA (Figure 1B). The intracellular nature of this interaction suggests that the biological consequence might be related to stress-responsive rather than immune-dependent functions of RelA. Within the context of cancer treatments, NF-κB-inducing stresses encountered by colorectal cancers include DNA-damaging chemotherapeutic agents (Barkett and Gilmore, 1999). We therefore decided to investigate endogenous intracellular C4BPA expression in two commonly used colorectal cancer cell lines (HCT 116 and RKO) treated with two standard-of-care chemotherapy agents: oxaliplatin and 5-fluorouracil (5-FU) (Pires et al., 2010). We found that both HCT 116 and RKO cells expressed endogenous C4BPA. Interestingly, in response to oxaliplatin, C4BPA protein levels were increased only in RKO cells. No major changes in protein expression were observed following 5-FU treatment (Figure 1C). In order to gain a better understanding of C4BPA's intracellular localization, we performed immunofluorescence experiments and found that C4BPA was distributed in the cytoplasm where C4BPA staining was found in the same areas as marked by tubulin (Figure S1A). Furthermore, for the most part, C4BPA did not colocalize with ER chaperone GRP78/BiP, suggesting that perinuclear C4BPA staining does not purely reflect production of the protein in the ER (Figure S1A). By performing subcellular fractionation experiments, we confirmed that intracellular C4BPA expression is primarily cytoplasmic in these cell lines and that oxaliplatin does not affect its subcellular localization (Figure 1D). Together these results indicate that intracellular C4BPA is mostly present in the cytoplasm. These data are consistent with our finding that C4BPA interacts with RelA even under unstressed conditions in which RelA would be mostly expected to be present in the cytoplasm (Karin and Lin, 2002). To our knowledge, this is the first report of intracellular C4BPA expression in cancer cells and of stress-dependent changes in C4BPA expression.

In RKO cells, which displayed oxaliplatin-induced C4BPA expression, we observed a decreased surviving fraction (compared to HCT 116 cells) particularly in response to oxaliplatin (Figure S1B). We also observed increased expression of the DNA Damage Response (DDR) marker, γH2AX and two pro-apoptotic markers, cleaved caspase 3 and Bax, as well as increased % apoptosis in RKO in response to oxaliplatin (Figure S1C and S1D). These data suggest that cells displaying elevated C4BPA expression become more susceptible to oxaliplatin-induced apoptosis. In order to validate this observation, we overexpressed C4BPA in HCT 116 cells. In line with our hypothesis, C4BPA overexpression resulted in increased apoptosis following oxaliplatin treatment (Figures 1E and S1E).

Intrigued by the differences in intracellular C4BPA expression and apoptosis sensitivity found between RKO and HCT 116 cells, we queried the *C4BPA* mutational status of these cells and noted that RKO colorectal cancer cells have a *C4BPA* missense mutation (c.1384G > A) while HCT 116 cells harbor wild-type (WT) *C4BPA*. In order to assess whether genetic alterations of *C4BPA* occur in patients' tumors, we queried The Cancer Genome Atlas (TCGA) data sets and found that *C4BPA* mutations and copy number alterations were present in a range of cancer types (when pan-cancer studies were queried) (Figure S1F). Interestingly, we found that there was a significant association of *C4BPA* mutation status and improved outcome when *C4BPA* mutations again were analyzed at the pan-cancer level (and corrected for type, age, and gender) (Figure 1F). We also noted that colorectal cancer was one example of several positive cancer types in which *C4BPA* mutations appeared to be associated with improved survival and this association remained even when corrected for age (Figures S1G and S1H and Table S1). In addition, C4BPA expression in tumors appeared significantly higher than in normal colon tissue (Figure S1I). The association with survival benefit in colorectal cancers harboring *C4BPA* mutations, however, did not correlate with immune response changes such as cytotoxic lymphocyte infiltration or increased cytolytic activity (recently found to be associated with improved survival) (Domingo et al., 2016). We found no significant changes in lymphocyte infiltration or cytolytic activity, suggesting that the association with improved survival is likely independent of these parameters (Figures S1J and S1K).

Consistent with the previously observed changes in apoptosis, when analyzing patient data by Gene Set Enrichment Analysis (GSEA) of TCGA RNA-seq data, we found that 'apoptosis' was the top differentially expressed pathway in colorectal cancer patients with *C4BPA* mutations (Figure 1G). Furthermore, analysis of proteins differentially expressed in *C4BPA*-mutant tumors (from TCGA reverse-phase protein array [RPPA] analysis data) followed by Gene Ontology analysis revealed that versions of 'regulation of apoptosis/cell death' also ranked as the top 3 enriched pathways (Figure 1H and Table S2) (Huang et al., 2008, 2009).

Since increased C4BPA expression and *C4BPA* mutations were both associated with increased apoptosis, we decided to further investigate the effect that patient-specific *C4BPA* mutations had on C4BPA expression levels.

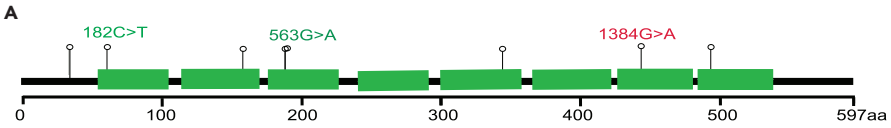

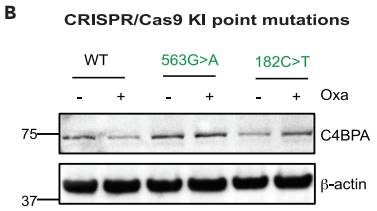

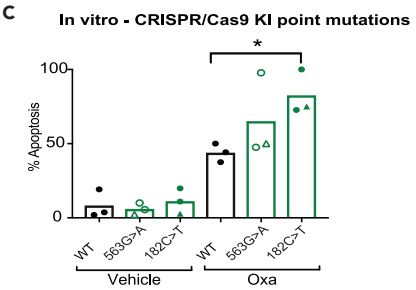

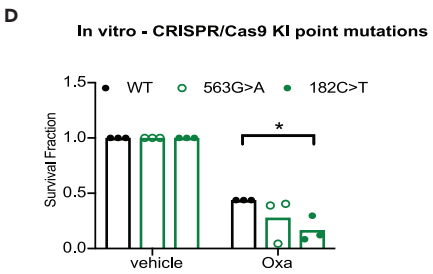

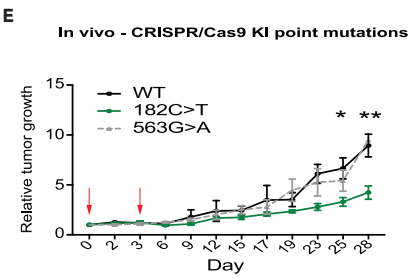

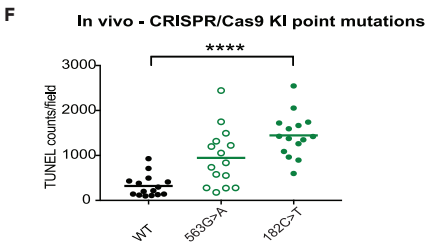

G

C4BPA status	WT	563G>A	182C>T
Δ in C4BPA expression	Decreased	No change	Increased
Apoptosis levels	Low	Intermediate	High

Figure 2. Patient-Specific *C4BPA*-Mutants Harbor Increased Intracellular C4BPA Expression and Apoptotic Signaling in Response to Oxaliplatin

(A) Schematic representation of *C4BPA* mutations identified by TCGA in the COADREAD data set as well as the *C4BPA* mutation found in RKO colorectal cancer cells (as reported in the Catalogue of Somatic Mutations in Cancer and shown in red text) (cancer.sager.ac.uk). Each lollipop represents a missense mutation. Mutations in green text represent those mutations tested further with the use of CRISPR knock-in cell lines. 182C > T, 563G > A and 1384G > A are highlighted since they are the endogenous mutants experimentally tested in this study. Figure adapted from cbiorportal.org.

(B) HCT 116 *C4BPA*^{WT}, HCT 116 *C4BPA*$^{563G>A}$ or HCT 116 *C4BPA*$^{182C>T}$ were treated with oxaliplatin (40 μM, 24 h). Western blotting was carried out with the antibodies indicated. β-Actin was used as the loading control. n = 3.

(C) HCT 116 *C4BPA*^{WT}, HCT 116 *C4BPA*$^{563G>A}$ or HCT 116 *C4BPA*$^{182C>T}$ were treated with oxaliplatin (40 μM, 24 h). The graph represents the number of apoptotic/non-apoptotic cells expressed as a % of the whole population. Two different clones are shown for each mutant (represented by different symbols). Individual dots represent values for each independent experiment. Statistical significance was evaluated by two-way ANOVA, * = $p < 0.05$ between WT Oxa and 182C > T Oxa. n = 3.

(D) Colony survival assay carried out following treatment of HCT 116 *C4BPA*^{WT}, HCT 116 *C4BPA*$^{563G>A}$, or HCT 116 C4BPA$^{182C>T}$ with either vehicle of oxaliplatin (80 μM, 1 h). Individual dots represent values for each independent

Figure 2. *Continued*

experiment (with three technical replicates per experiment). Statistical significance was evaluated by two-way ANOVA, * = $p < 0.05$ between WT Oxa and 182C > T Oxa. n = 3.

(E) HCT 116 *C4BPA*^{WT,} HCT 116 *C4BPA*$^{563G>A}$, or HCT 116 *C4BPA*$^{182C>T}$ cells were injected subcutaneously into athymic nude female mice. Growing tumors were treated with oxaliplatin (10 mg/kg) once tumors reached an average size of 60–90 mm^3 (labeled day 0). Treatment was repeated on day 3. Red arrows indicate day of oxaliplatin treatment. n = 7–9 mice per group. Statistical significance was evaluated by two-way ANOVA, * = $p < 0.05$. Error bars represent the standard error of the mean.

(F) Apoptosis was assessed by Terminal deoxynucleotidyl transferase dUTP Nick-End Labeling (TUNEL) staining in sections from HCT 116 *C4BPA*^{WT}, HCT 116 *C4BPA*$^{563G>A}$, or HCT 116 *C4BPA*$^{182C>T}$ xenografts treated with oxaliplatin as in (E). Graph represents the number of TUNEL-positive cells per field of view in 2–4 tumors per xenograft model. Statistical significance was evaluated by two-way ANOVA, **** = $p < 0.0001$ between WT and 182C > T.

(G) Table describing the rationale behind the selection of *C4BPA* mutants generated by CRISPR/Cas9 technology and the summary of C4BPA expression changes (Δ) and apoptosis level observed upon oxaliplatin treatment.

See also Figure S2.

To this end, we transfected *C4BPA*-mutant expression vectors into HCT 116 cells (with previously depleted endogenous C4BPA). When assessing C4BPA intracellular expression in this system, we noted that C4BPA was localized predominantly in the cytoplasm in *C4BPA* WT cells (as also shown in Figures 1D and S1A) and that *C4BPA* mutations did not alter this localization (Figure 1I). Importantly, as was observed in our initial experiments using *C4BPA* WT (HCT 116) and *C4BPA*-mutant (RKO) cells (Figure 1C), intracellular C4BPA expression in response to oxaliplatin treatment was only increased in cells harboring *C4BPA* mutations (Figure 1I).

Patient-Specific *C4BPA* Mutants Harbor Increased Intracellular C4BPA Expression and Apoptotic Signaling in Response to Oxaliplatin

In order to gain deeper insight into whether increased intracellular C4BPA could regulate the observed changes in apoptosis, we decided to generate CRISPR knock-in (KI) mutant cell lines harboring different *C4BPA* mutations found in tumors from patients with colorectal cancer (Figures 2A and S2A). Generation of these cell lines, we reasoned, would allow us to test, in an endogenous setting: 1) the effects of *C4BPA* mutations on changes in C4BPA protein expression; and 2) whether increases in intracellular C4BPA levels affect apoptotic signaling. We generated a cell line harboring the 182C > T mutation (cells referred to as HCT 116 *C4BPA*$^{182C>T}$) since we previously observed a marked induction of C4BPA protein levels following oxaliplatin treatment in cells overexpressing this mutant (Figure 1I). We also generated a cell line harboring the 563G > A mutation (cells referred to as HCT 116 *C4BPA*$^{563G>A}$) since cells overexpressing this mutant showed high baseline C4BPA expression and minimal further increased C4BPA protein expression following oxaliplatin treatment (Figure 1I). HCT 116 *C4BPA*$^{182C>T}$ cells, we reasoned, would provide a representative model for increased expression of endogenous intracellular C4BPA, while cell line HCT 116 *C4BPA*$^{563G>A}$ could serve as a direct control since this mutant does not associate with increased intracellular C4BPA expression upon oxaliplatin treatment. In support of data shown in Figure 1I, both CRISPR KI cell lines showed high levels of C4BPA following oxaliplatin treatment compared to the WT cells, with the greatest increase in C4BPA expression observed in HCT 116 *C4BPA*$^{182C>T}$ cells (Figure 2B). As expected, HCT 116 *C4BPA*$^{563G>A}$ cells displayed high levels of C4BPA even under basal conditions, and oxaliplatin treatment caused only minimal further increase (Figure 2B).

Surprisingly, intracellular protein expression levels did not correlate with changes in mRNA levels in either WT or mutant cell lines (Figure S2B). In addition, C4BPA mRNA expression levels in patients harboring *C4BPA* mutations were not significantly different from that of patients without mutations (Figure S2C). Together, these data suggest that transcriptional changes alone cannot explain the observed changes in intracellular expression. Increased C4BPA protein expression in cell lysates from *C4BPA*-mutant cell lines, however, correlated with a decrease in C4BPA secretion into conditioned media following oxaliplatin treatment in two different *C4BPA*-mutant model systems (Figures S2D and S2E). These data suggest that the observed increased intracellular expression could result from either decreased secretion in the cells harboring sensitive *C4BPA* mutations or alternatively, an increased uptake of secreted protein. Interestingly, no signs of increased ER stress marker BiP were observed in our mutants compared to *C4BPA* WT cells (even when treated with tunicamycin and oxaliplatin), suggesting that increased intracellular accumulation of C4BPA does not lead to increased ER stress (Figure S2F).

Next, we used our CRISPR KI cells as tools to understand the effects of oxaliplatin-induced intracellular C4BPA protein expression on apoptosis sensitivity in further detail. When these cell lines were tested *in vitro*, HCT 116 *C4BPA*$^{182C>T}$ displayed elevated levels of apoptosis compared to WT control (HCT 116

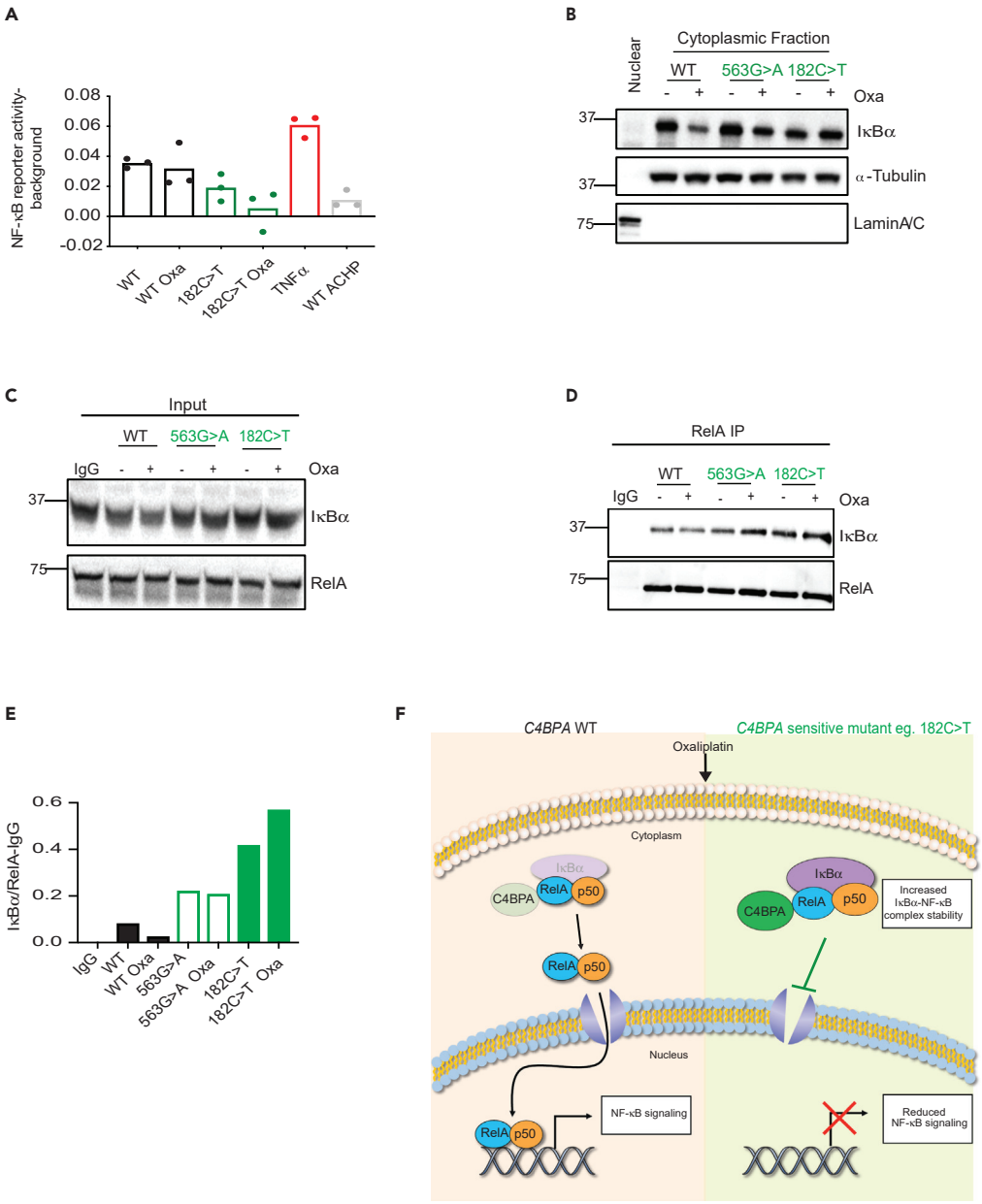

Figure 3. Patient-Specific C4BPA Mutants Display Decreased NF-κB Signaling

(A) HCT 116 *C4BPA*^{WT}, HCT 116 *C4BPA*$^{563G>A}$, or HCT 116 *C4BPA*$^{182C>T}$ were treated with oxaliplatin (40 μM, 24 h) or vehicle. Treatment of HCT 116 *C4BPA*^{WT} with TNF-α was used as a positive control. Treatment of HCT 116 *C4BPA*^{WT} with IκB kinase inhibitor ACHP (25 μM) was used as a negative control. NF-κB reporter assay was carried out. NF-κB reporter luciferase activity – background renilla is shown.

(B) Cellular fractionation to separate nuclear and cytoplasm fractions followed by western blotting was carried out in HCT 116 *C4BPA*^{WT}, HCT 116 *C4BPA*$^{563G>A}$, or HCT 116 *C4BPA*$^{182C>T}$ cells treated with oxaliplatin (40 μM, 24 h). α-Tubulin was used as a control for the cytoplasmic fraction, and LaminA/C was used as the nuclear control. n = 3. Nuclear fraction is shown in the first lane as control.

(C and D) HCT 116 *C4BPA*^{WT}, HCT 116 *C4BPA*$^{563G>A}$, or HCT 116 *C4BPA*$^{182C>T}$ cells were transfected with either WT *C4BPA* or mutant *C4BPA* (563G > A or 182C > T, respectively). Pull-down with RelA antibody was performed, and the input and IP for those experiments is shown. Input was collected from the same experiment as IP. Western blotting was carried out with the antibodies indicated. n = 2. IgG control is shown in the left lane of the blot.

(E) Quantification of IκBα/RelA relative abundance as shown in the western blot in (D).

Figure 3. *Continued*
(F) Proposed Model: Cells harboring 'sensitive' *C4BPA* mutations (eg *C4BPA*$^{182C>T}$) have increased oxaliplatin-induced expression of intracellular C4BPA and cytoplasmic expression of IκBα which are associated with increased retention of IκBα-NF-κB inhibitory complexes and a subsequent attenuated NF-κB signaling. These effects correlate with oxaliplatin-induced apoptosis sensitivity and *in vivo* oxaliplatin tumor response as shown in Figure 2.
See also Figure S3.

cells with no *C4BPA* mutation) or HCT 116 *C4BPA*$^{563G>A}$ cells (Figure 2C). HCT 116 *C4BPA*$^{182C>T}$ cells also displayed the greatest decreased viability in response to oxaliplatin in clonogenic assays (Figures 2D and S2G). These data are in line with our hypothesis that increased C4BPA intracellular expression following oxaliplatin treatment contributes to increased apoptosis and oxaliplatin sensitivity. Furthermore, xenografts from HCT 116 *C4BPA*$^{182C>T}$ cells displayed a significant tumor growth delay and increased apoptosis following treatment with oxaliplatin compared to WT control or HCT 116 *C4BPA*$^{563G>A}$ (Figure 2E, 2F, and S2H). These data support the importance of intracellular C4BPA expression and its correlation with apoptosis sensitivity and improved oxaliplatin tumor response in specific *C4BPA*-mutant backgrounds. A table describing the rationale behind the selection of *C4BPA* mutants generated by CRISPR/Cas9 technology and the summary of C4BPA expression and apoptosis level changes observed upon oxaliplatin treatment is shown in Figure 2G.

Patient-Specific *C4BPA* Mutants Display Decreased NF-κB Signaling

Since NF-κB activation can reduce chemosensitivity by promoting an anti-apoptotic transcriptional response, we hypothesized that an interaction between C4BPA and RelA could regulate oxaliplatin-induced apoptosis by altering NF-κB anti-apoptotic signaling (Barkett and Gilmore, 1999). In support of this hypothesis, cells with the greatest levels of oxaliplatin-induced apoptosis and intracellular C4BPA expression (HCT 116 *C4BPA*$^{182C>T}$) displayed reduced NF-κB reporter activity. Remarkably, NF-κB reporter activity in this mutant cell line was reduced to levels comparable to those of WT cells treated with an IκB kinase pharmacological inhibitor (ACHP) (used as a negative control). NF-κB inducer, TNFα, was used as positive control in these experiments (Figure 3A). Decreased NF-κB activity could be a result of aberrant expression or stabilization of NF-κB inhibitor, IκB, upon oxaliplatin treatment. Indeed, while *C4BPA* WT cells showed a strong reduction in cytoplasmic IκBα levels upon oxaliplatin treatment, this reduction was attenuated in the mutants. HCT 116 *C4BPA*$^{182C>T}$ cells that show the greatest apoptosis sensitivity, largest increase in C4BPA expression, and least NF-κB activity showed no decrease in IκBα levels upon treatment (Figure 3B).

These data suggest that in certain *C4BPA*-mutant backgrounds (such as the *C4BPA*$^{182C>T}$ alteration), the activity of DNA-binding NF-κB proteins (such as RelA) is impaired, likely due to the increased expression of the inhibitory NF-κB protein IκBα. Importantly, we observed increased binding of IκBα to RelA following oxaliplatin treatment in *C4BPA* mutants, with the most significant increase in IκBα-RelA complex stability observed, as expected, in HCT 116 *C4BPA*$^{182C>T}$ cells (Figures 3C–3F).

Increased IκBα Expression in *C4BPA*-Mutant Cell Lines Is Associated with Increased Translation Markers

IκBα undergoes proteasomal degradation following phosphorylation by IKK kinases (Chen et al., 2000; Karin and Lin, 2002). Thus, changes in IκBα stability in *C4BPA*-mutant cell lines could result from differences in expression of IKK kinases or IκBα phosphorylation. However, we did not observe any decreased expression of the catalytic subunit of the IKK complex, IKKα in *C4BPA*-mutant cells, which also displayed robust IκBα phosphorylation (Figures S3A and S3B). In addition, while significant increases in mRNA levels of IκBα were observed in HCT 116 *C4BPA*^{WT} and HCT 116 *C4BPA*$^{563G>A}$ cell lines, increased IκBα mRNA levels did not reach significance in HCT 116 *C4BPA*$^{182C>T}$ cells, indicating that transcriptional changes are also unlikely to be the main contributors to the increased protein IκBα levels observed in these cells (Figures S3C–S3E). Of note, since IκBα itself is thought to be an NF-κB target, the lack of significant increased IκBα expression in HCT 116 *C4BPA*$^{182C>T}$ cells is in line with decreased NF-κB activity in this cell line as shown in Figure 3A (Sun et al., 1993). Inhibition of protein synthesis has also been shown to activate NF-κB activity by modulating the synthesis of IκB proteins (O'Dea et al., 2007). We assessed levels of protein translation marker, phosphorylated 4E-BP1 (p4E-BP1), in *C4BPA* WT and *C4BPA*-mutant cell lines. Cells harboring *C4BPA*-mutants (as well as WT overexpression) displayed increased levels of translation marker p4E-BP1, particularly under unstimulated conditions (Figures S3F–S3H). Once again, this phenotype

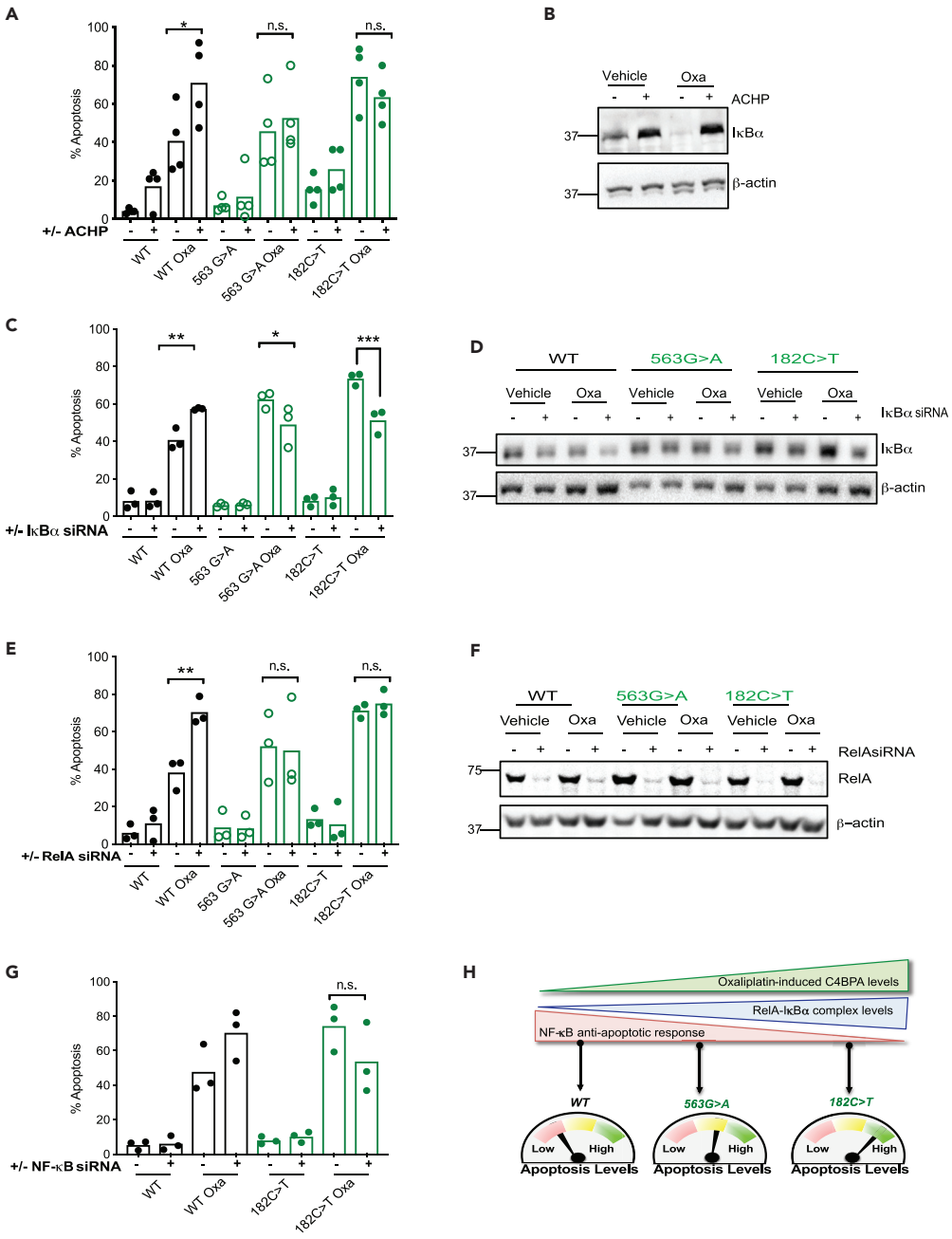

Figure 4. Altered NF-κB Signaling Regulates Apoptosis in Patient-Specific *C4BPA*-Mutant Backgrounds

(A) HCT 116 *C4BPA*^{WT}, HCT 116 *C4BPA*$^{563G>A}$, or HCT 116 *C4BPA*$^{182C>T}$ cells were treated with either DMSO or IκB kinase inhibitor ACHP (25 μM) and oxaliplatin (40 μM, 24 h). The graph represents the number of apoptotic/non-apoptotic cells expressed as a % of the whole population. Individual dots represent mean values for each independent experiment, n = 3–4. Statistical significance was evaluated by two-way ANOVA, **** = $p < 0.0001$. * = $p < 0.05$.

(B) HCT 116 *C4BPA*^{WT} cells were treated with either DMSO or ACHP (25 μM) and oxaliplatin (40 μM, 24 h). Western blotting was carried out with the antibodies indicated. β-Actin was used as the loading control. n = 3. ACHP results in stabilization of IκBα as expected.

(C) HCT 116 *C4BPA*^{WT}, HCT 116 *C4BPA*$^{563G>A}$, or HCT 116 *C4BPA*$^{182C>T}$ cells were transfected with either scramble (Scr) or IκBα siRNA and treated with oxaliplatin (40 μM, 24 h). The graph represents the number of apoptotic/non-apoptotic cells expressed as a % of the whole population. Individual dots represent mean values for each independent experiment. Statistical significance was evaluated by two-way ANOVA, * = $p < 0.05$, ** = $p < 0.01$, *** = $p < 0.001$. n = 3.

Figure 4. *Continued*

(D) HCT 116 *C4BPA*^{WT}, HCT 116 *C4BPA*$^{563G>A}$, or HCT 116 *C4BPA*$^{182C>T}$ cells were transfected with either scramble (Scr) or IκBα siRNA and treated with oxaliplatin (40 μM, 24 h). Western blotting was carried out with the antibodies indicated. β-Actin was used as the loading control. n = 3.

(E) HCT 116 *C4BPA*^{WT}, HCT 116 *C4BPA*$^{563G>A}$, or HCT 116 *C4BPA*$^{182C>T}$ cells were transfected with either Scr or RelA siRNA and treated with oxaliplatin (40 μM, 24 h). The graph represents the number of apoptotic/non-apoptotic cells expressed as a % of the whole population. Individual dots represent mean values for each independent experiment. Statistical significance was evaluated by two-way ANOVA, * = $p < 0.05$. n = 3.

(F) HCT 116 *C4BPA*^{WT}, HCT 116 *C4BPA*$^{563G>A}$, or HCT 116 *C4BPA*$^{182C>T}$ cells were transfected with either Scr or RelA siRNA and treated with oxaliplatin (40 μM, 24 h). Western blotting was carried out with the antibodies indicated. β-Actin was used as the loading control. n = 3.

(G) HCT 116 C4BPA^{WT}, or HCT 116 C4BPA$^{182C>T}$ cells were transfected with either Scr or NF-κB1 siRNA and treated with oxaliplatin (40 μM, 24 h). Individual dots represent mean values for each independent experiment. n = 3. Statistical significance was evaluated by two-way ANOVA, **$p < 0.01$.

(H) Proposed Model: Increasing stabilization of intracellular C4BPA correlates with increased cytoplasmic IκBα and increased retention of RelA-IκBα in inhibitory complexes. These responses are particularly prominent in *C4BPA*-mutant cell lines most sensitive to oxaliplatin-induced apoptosis (eg *C4BPA*$^{182C>T}$). In contrast, when C4BPA levels are low (such as in a WT setting), decreased cytoplasmic IκBα results in reduced retention of NF-κB in inhibitory complexes following oxaliplatin treatment and reduced apoptosis levels. A mutant with no C4BPA stabilization (*C4BPA*$^{563G>A}$) following oxaliplatin treatment shows an intermediate apoptotic response correlating with intermediate levels of RelA-IκBα retained in inhibitory complexes.

See also Figure S4.

appeared particularly marked in cells harboring the most sensitive mutant, *C4BPA*$^{182C>T}$. In order to interrogate whether altered protein synthesis was contributing to increased IκBα protein levels, we used translation inhibitor cycloheximide (CHX). CHX blockade experiments suggest that IκBα levels can be regulated at the translational level in *C4BPA*-mutant cell lines with CHX treatment reducing IκBα protein expression back to WT levels (Figure S3I).

Altered NF-κB Signaling Regulates Apoptosis in Patient-Specific *C4BPA*-Mutant Backgrounds

Our data suggest that increased IκBα levels regulate NF-κB signaling in *C4BPA* mutants through regulation of IκBα-RelA cytoplasmic retention. In order to test whether cytoplasmic retention of NF-κB inhibitory complexes was mediating the increased apoptosis, we used IκB kinase inhibitor, ACHP, which prevents nuclear translocation of NF-κB complexes due to increased IκBα stability (Figures 4A and 4B). We hypothesized that treatment with ACHP should lead to the most pronounced increase in apoptosis levels in WT cells and that no further increase in apoptosis levels would be observed in the most sensitive C4BPA mutants (*C4BPA*$^{182C>T}$) owing to the fact that nuclear translocation of NF-κB complexes is likely already impaired in these cells. In support of our hypothesis, treatment with this inhibitor showed that stabilization of IκBα complexes only caused a notable increase of apoptosis in the WT background. These data support our hypothesis that, in *C4BPA*-mutant backgrounds, the activity of DNA-binding NF-κB proteins is impaired by the increased expression of inhibitory proteins, likely retaining transcriptionally active RelA in inhibitory complexes. As expected, further inhibition of nuclear translocation by ACHP had therefore no additional effect on apoptosis induction in these mutants. To formally test the role of IκBα in apoptotic signaling, we depleted IκBα and assessed apoptosis levels in *C4BPA* WT or *C4BPA*-mutant cell lines. We reasoned that depletion of IκBα would relieve some of the inhibition on NF-κB signaling and 'rescue' apoptosis levels in *C4BPA*$^{182C>T}$-mutant cells to levels comparable to *C4BPA*^{WT} cells. As expected, reduction of IκBα levels (to protein levels comparable to those found in *C4BPA*^{WT}) resulted in decreased apoptosis in *C4BPA*$^{182C>T}$-mutant cells to levels comparable to *C4BPA*^{WT} cells treated with Scr siRNA (Figures 4C and 4D). These data suggest that under conditions of increased C4BPA intracellular expression, the activity of DNA-binding NF-κB proteins is particularly impaired due to the increased expression of inhibitory NF-κB proteins.

Finally, to assess the role of NF-κB-DNA-binding family members in regulating apoptosis in *C4BPA* mutants, we evaluated apoptosis following depletion of the DNA-binding NF-κB family members originally identified as C4BPA predicted functional partners by STRING (Figure 1A). In these experiments, we again used our CRISPR KI cells lines as tools to understand the effects of NF-κB family member depletion in cells displaying varying levels of oxaliplatin-induced intracellular C4BPA protein expression. We hypothesized that in those cells with the greatest increases in oxaliplatin-induced C4BPA levels, apoptotic sensitivity and attenuated NF-κB anti-apoptotic responses (such as HCT 116 *C4BPA*$^{182C>T}$) depletion of RelA/NF-

κB1 would result in minimal additional changes to apoptosis levels. In support of our hypothesis, no changes in apoptosis were observed following RelA depletion in *C4BPA*-mutant cell line HCT 116 *C4BPA*$^{182C>T}$ (Figures 4E and 4F). These results were supported by experiments using NF-κB1 siRNA (Figures 4G and S4A). In contrast, as expected, RelA/NF-κB1 depletion experiments showed a marked increase in apoptosis following oxaliplatin treatment in HCT 116 *C4BPA*^{WT} cells (Figures 3A and 3B). HCT 116 *C4BPA*$^{563G>A}$ cells were used as a control in RelA depletion experiments. As had been previously observed, apoptosis in these cells never reached the high levels observed in HCT 116 *C4BPA*$^{182C>T}$ cells and instead remained at an intermediate level between HCT 116 *C4BPA*^{WT} and *C4BPA*$^{182C>T}$ cells (Figure 4E). These data are in line with the lack of oxaliplatin-induced C4BPA expression in these cells. These data further support our hypothesis that cells with increased C4BPA protein expression following oxaliplatin treatment display increased apoptosis due to impaired or inhibited NF-κB signaling.

Together these results highlight the importance of studying mutations in innate immunity-associated genes as a tool to uncover novel functions. Using this approach, we identify that C4BPA has cancer-associated functions that are distinct from its canonical role in the complement system. Specifically, we reveal that C4BPA functions as a 'rheostat,' regulating oxaliplatin-induced apoptosis through modulation of NF-κB signaling (Figure 4H).

DISCUSSION

Innate immunity-associated proteins with intracellular functions, such as TREX1, cGas, and STING, are emerging as important contributors to treatment response and tumor progression (Cai et al., 2014; Vanpouille-Box et al., 2017; Dunphy et al., 2018; Liu et al., 2018). However, despite the rising interest in tumor cell-intrinsic functions for innate immunity-associated proteins, there is a lack of studies investigating the intracellular roles of extracellular innate immunity-associated proteins and what regulates their intracellular expression.

Here, we show that C4BPA is expressed intracellularly in a stress-responsive and mutation-dependent manner. Using the study of specific *C4BPA* mutations found in patients, we uncover an unexpected, likely immune-independent function for C4BPA. Experimentally, *in vitro* and/or *in vivo*, we show that intracellular C4BPA expression in different *C4BPA*-mutant backgrounds appears to function as a 'rheostat,' tipping the balance toward increased apoptosis following oxaliplatin treatment. In these experiments, cells harboring *C4BPA* mutation (563G > A), with minimal increased stress-responsive C4BPA intracellular expression, as expected, displayed a weaker apoptotic response and tumor regression *in vivo* than a sensitive mutation (182C > T) displaying increased stress-responsive C4BPA intracellular expression. These data are in line with increased C4BPA intracellular expression tipping the balance toward increased apoptosis. It is important to note, however, that while cells harboring *C4BPA* mutation (563G > A) displayed a lower apoptotic response than those harboring sensitive *C4BPA* mutation (182C > T), these cells still showed a trend toward increased apoptosis in comparison to WT cells. These data probably reflect the fact that C4BPA levels following oxaliplatin treatment in these cells remained higher than those of WT cells.

Mechanistically, we show that the increased apoptosis observed in oxaliplatin-sensitive *C4BPA* mutants is associated with attenuated NF-κB-dependent anti-apoptotic responses. We propose that in cells with increased stress-responsive C4BPA intracellular expression, transcriptionally active NF-κB proteins are impaired due to the elevated expression levels of NF-κB inhibitory proteins. Indeed, following oxaliplatin treatment, we observed increased expression of cytoplasmic inhibitory NF-κB protein, IκBα, in sensitive *C4BPA*-mutant cells as well as increased IκBα-RelA complexes. These cells also displayed decreased NF-κB reporter activity. We propose that increased C4BPA protein levels following oxaliplatin treatment could contribute to increased stability of IκBα-RelA complexes.

Links between NF-κB activation and complement, specifically C3, have been recently suggested in the context of Alzheimer's disease and viral and bacterial infections (Lian et al., 2014; Tam et al., 2014). However, no associations between these two pathways and how they may cooperate to regulate apoptosis have been suggested in a cancer context, which likely reflects the fact that intracellular roles for complement proteins have only recently been considered (Liszewski et al., 2013; Arbore et al., 2017; Elvington et al., 2017; Kremlitzka et al., 2019). Of note, a recent study reported that complement factor properdin may act as a tumor suppressor in breast cancer models by upregulating ER-activated pro-apoptotic transcription factor *DDIT3* (Block et al., 2019). Furthermore, Complement C1q-Binding Protein (C1QBP) was recently

shown to play an important role in the DNA damage response by binding, stabilizing, and controlling MRE11's nuclease activity (Bai et al., 2019). These studies, like ours, highlight the importance of investigating intracellular functions of complement proteins.

Interestingly, C4BP can bind DNA mainly through a patch of positively charged amino acids on C4BPA (Trouw et al., 2005). We did not investigate the DNA binding capabilities of C4BPA in our models. However, given that intracellular C4BPA is primarily localized in the cytoplasmic/extranuclear space, it would be interesting to investigate whether C4BPA can bind cytosolic nucleic acids in future studies. Since the environment of the cytoplasm is distinct from that of the extracellular space, it is possible that the structural features of intracellular C4BPA might be different from those of C4BPA present extracellularly (López-Mirabal and Winther, 2008). Interestingly, Hofmeyer et al. reported that the C4BPA heptamer is very stable due to a large number of hydrophobic interactions and formation of electrostatic, disulfide, and hydrogen bonds (Hofmeyer et al., 2013). Whether intracellular C4BPA is present as a single chain or multimer was not investigated in this study. However, it is possible that, even if disulfide bonds are not formed efficiently intracellularly, C4BPA might still be present in a multimeric form as occurs in the main C4BP isoform.

Overall our study provides the first description of stress-specific and mutation-dependent intracellular induction of C4BPA expression in cancer cells and describes the importance of the interplay between C4BPA and NF-κB in regulating oxaliplatin-induced apoptosis sensitivity in colorectal cancer.

Limitations of the Study

Here we uncover that, in colorectal cancer cells, C4BPA has an intracellular role in the regulation of apoptosis following oxaliplatin treatment. Future studies should test a wider range of DNA-damaging agents and cell types. Similarly, testing the effect of *C4BPA* mutations on tumor progression and treatment response in other tumor models would be interesting, given that *C4BPA* mutations are associated with improved survival in all epithelial cancer types queried. By studying patient-specific *C4BPA* mutations, we have focused on the description of an unexpected non-canonical function for C4BPA but have not investigated whether these mutations can impact canonical complement regulation. Furthermore, whether intracellular C4BPA interacts with its canonical ligand/binding partners intracellularly remains to be formally tested. Of note, expression of C4 and C4BPB in the colorectal cancer cell lines used in this study is very low ([Roumenina et al., 2019] and https://www.ebi.ac.uk). We cannot rule out, however, that extracellular C4 or C4BPB could interact with intracellular C4BPA if taken into the cell.

Resource Availability

Lead Contact

Monica M. Olcina (monica.olcinadelmolino@uzh.ch).

Materials Availability

Further information and requests for resources and reagents should be directed to and will be fulfilled by the Lead Contact Monica M. Olcina (monica.olcinadelmolino@uzh.ch).

Data and Code Availability

The published article includes all data sets/code generated or analyzed during this study.

METHODS

All methods can be found in the accompanying Transparent Methods supplemental file.

SUPPLEMENTAL INFORMATION

Supplemental Information can be found online at https://doi.org/10.1016/j.isci.2020.101594.

ACKNOWLEDGMENTS

This work was supported by NIH Grants CA-67166 and CA-197713, the Silicon Valley Foundation, the Sydney Frank Foundation, and the Kimmelman Fund (A.J.G.). M.M.O. was a Cancer Research Institute Irvington

Fellow supported by the Cancer Research Institute and Stiftung für Forschung, Medical Faculty, UZH. R.K.K. was supported by Stanford ChEM-H Undergraduate Scholars Program. T.G.G. was supported by the NCI/NIH (P01 CA168585) and an American Cancer Society Research Scholars Grant. M.S. and M.M.O. were supported by a project grant from the Swiss National Foundation (31003A_163141).

AUTHOR CONTRIBUTIONS

Conceptualization, M.M.O and A.J.G. Methodology M.M.O, R.K.K and C.G.L. Writing original draft, M.M.O. Writing review and editing, M.M.O, A.J.G, N.G.B, C.G.K and D.R. Investigation, M.M.O, R.K.K and C.G.L. Formal analysis, M.M.O, N.G.B and R.V.E. Resources, A.J.G, T.G.G and M.S. Supervision M.M.O and A.J.G. Funding acquisition, M.M.O, A.J.G, T.G.G ad M.S.

DECLARATION OF INTERESTS

The authors declare no competing interests.

Received: March 25, 2020
Revised: August 11, 2020
Accepted: September 17, 2020
Published: October 23, 2020

REFERENCES

Arbore, G., Kemper, C., and Kolev, M. (2017). Intracellular complement – the complosome – in immune cell regulation. Mol. Immunol. *89*, 2–9.

Bai, Y., Wang, W., Li, S., Zhan, J., Li, H., Zhao, M., Zhou, X.A., Li, S., Li, X., Huo, Y., et al. (2019). C1QBP promotes homologous recombination by stabilizing MRE11 and controlling the assembly and activation of MRE11/RAD50/NBS1 complex. Mol. Cell *75*, 1299.

Barkett, M., and Gilmore, T.D. (1999). Control of apoptosis by Rel/NF-kappaB transcription factors. Oncogene *18*, 6910–6924.

Block, I., Müller, C., Sdogati, D., Pedersen, H., List, M., Jaskot, A.M., Syse, S.D., Lund Hansen, P., Schmidt, S., Christiansen, H., et al. (2019). CFP suppresses breast cancer cell growth by TES-mediated upregulation of the transcription factor DDIT3. Oncogene *38*, 4560.

Cai, X., Chiu, Y.H., and Chen, Z.J. (2014). The cGAS-cGAMP-STING pathway of cytosolic DNA sensing and signaling. Mol. Cell *54*, 289–296.

Chen, C., Edelstein, L.C., and Gelinas, C. (2000). The rel/NF-kappa B family directly activates expression of the apoptosis inhibitor Bcl-xL. Mol. Cell. Biol. *20*, 2687–2695.

Domingo, E., Freeman-Mills, L., Rayner, E., Glaire, M., Briggs, S., Vermeulen, L., Fessler, E., Medema, J.P., Boot, A., Morreau, H., et al. (2016). Somatic POLE proofreading domain mutation, immune response, and prognosis in colorectal cancer: a retrospective, pooled biomarker study. Lancet Gastroenterol. Hepatol. *1*, 207–216.

Dunphy, G., Flannery, S.M., Almine, J.F., Connolly, D.J., Paulus, C., Jønsson, K.L., Jakobsen, M.R., Nevels, M.M., Bowie, A.G., and Unterholzner, L. (2018). Non-canonical activation of the DNA sensing adaptor STING by ATM and IFI16 mediates NF-κB signaling after nuclear DNA damage. Mol. Cell *71*, 745.

Elvington, M., Liszewski, M.K., Bertram, P., Kulkarni, H.S., and Atkinson, J.P. (2017). A C3(H20) recycling pathway is a component of the intracellular complement system. J. Clin. Invest. *127*, 970–981.

Hoesel, B., and Schmid, J.A. (2013). The complexity of NF-κB signaling in inflammation and cancer. Mol. Cancer *12*, 86.

Hofmeyer, T., Schmelz, S., Degiacomi, M.T., Dal Peraro, M., Daneschdar, M., Scrima, A., van den Heuvel, J., Heinz, D.W., and Kolmar, H. (2013). Arranged sevenfold: structural insights into the C-terminal oligomerization domain of human C4b-binding protein. J. Mol. Biol. *425*, 1302.

Huang, D.W., Sherman, B.T., and Lempicki, R.A. (2008). Systematic and integrative analysis of large gene lists using DAVID bioinformatics resources. Nat. Protoc. *4*, 44–57.

Huang, D.W., Sherman, B.T., and Lempicki, R.A. (2009). Bioinformatics enrichment tools: paths toward the comprehensive functional analysis of large gene lists. Nucleic Acids Res. *37*, 1–13.

Karin, M., and Lin, A. (2002). NF-kappaB at the crossroads of life and death. Nat. Immunol. *3*, 221–227.

Kremlitzka, M., Nowacka, A.A., Mohlin, F.C., Bompada, P., De Marinis, Y., and Blom, A.M. (2019). Interaction of serum-derived and internalized C3 with DNA in human B cells-a potential involvement in regulation of gene transcription. Front. Immunol. *10*, 493.

Legrand, A.J., Konstantinou, M., Goode, E.F., and Meier, P. (2019). The diversification of cell death and immunity: memento mori. Mol. Cell *76*, 232.

Lian, H., Yang, L., Cole, A., Sun, L., Chiang, A.C., Fowler, S.W., Shim, D.J., Rodriguez-Rivera, J., Taglialatela, G., Jankowsky, J.L., et al. (2014). NFκB-Activated astroglial release of complement C3 compromises neuronal morphology and function associated with Alzheimer's disease. Neuron *85*, 101–115.

Liszewski, M.K., Kolev, M., Le Friec, G., Leung, M., Bertram, P.G., Fara, A.F., Subias, M., Pickering, M.C., Drouet, C., Meri, S., et al. (2013). Intracellular complement activation sustains T cell homeostasis and mediates effector differentiation. Immunity *39*, 1143–1157.

Liu, H., Zhang, H., Wu, X., Ma, D., Wu, J., Wang, L., Jiang, Y., Fei, Y., Zhu, C., Tan, R., et al. (2018). Nuclear cGAS suppresses DNA repair and promotes tumorigenesis. Nature *563*, 131.

López-Mirabal, H.R., and Winther, J.R. (2008). Redox characteristics of the eukaryotic cytosol. Biochim. Biophys. Acta *1783*, 629.

MacKenzie, K.J., Carroll, P., Martin, C.A., Murina, O., Fluteau, A., Simpson, D.J., Olova, N., Sutcliffe, H., Rainger, J.K., Leitch, A., et al. (2017). CGAS surveillance of micronuclei links genome instability to innate immunity. Nature *548*, 461–465.

O'Dea, E.L., Barken, D., Peralta, R.Q., Tran, K.T., Werner, S.L., Kearns JD, Levchenko, A., and Hoffmann, A. (2007). A homeostatic model of IκB metabolism to control constitutive NF-κB activity. Mol. Syst. Biol. *3*, 111.

Olcina, M.M., Balanis, N.G., Kim, R.K., Aksoy, B.A., Kodysh, J., Thompson, M.J., Hammerbacher, J., Graeber, T.G., and Giaccia, A.J. (2018). Mutations in an innate immunity pathway are associated with poor overall survival outcomes and hypoxic signaling in cancer. Cell Rep. *25*, 3721–3732.e6.

Pires, I.M., Ward, T.H., and Dive, C. (2010). Oxaliplatin responses in colorectal cancer cells are modulated by CHK2 kinase inhibitors. Br. J. Pharmacol. *159*, 1326–1338.

Reis, E.S., Mastellos, D.C., Ricklin, D., Mantovani, A., and Lambris, J.D. (2017). Complement in cancer: untangling an intricate relationship. Nat. Rev. Immunol. https://doi.org/10.1038/nri.2017.97.

Ricklin, D., Reis, E.S., and Lambris, J.D. (2016). Complement in disease: a defence system turning offensive. Nat. Rev. Nephrol. *12*, 383.

Roumenina, L.T., Daugan, M.V., Noe, R., Petitprez, F., Vano, Y.A., Sanchez-Salas, R., Becht, E., Meilleroux, J., Le Clec'h, B., Giraldo, N.A., et al. (2019). Tumor cells hijack macrophage-produced complement C1q to promote tumor growth. Cancer Immunol. Res. https://doi.org/10.1158/2326-6066.CIR-18-0891.

Sayegh, E.T., Bloch, O., and Parsa, A.T. (2014). Complement anaphylatoxins as immune regulators in cancer. Cancer Med. *3*, 747–758.

Sun, S., Ganchi, P., Ballard, D., and Greene, W. (1993). NF-κB controls expression of inhibitor IκBα: evidence for an inducible autoregulatory pathway. Science *259*, 1912.

Tam, J.C., Bidgood, S.R., McEwan, W.A., and James, L.C. (2014). Intracellular sensing of complement C3 activates cell autonomous immunity. Science *345*, 1256070.

Trouw, L.A., Nilsson, S.C., Gonçalves, I., Landberg, G., and Blom, A.M. (2005). C4b-binding protein binds to necrotic cells and DNA, limiting DNA release and inhibiting complement activation. J. Exp. Med. *201*, 1937.

Vanpouille-Box, C., Alard, A., Aryankalayil, M.J., Sarfraz, Y., Diamond, J.M., Schneider, R.J., Inghirami, G., Coleman, C.N., Formenti, S.C., and Demaria, S. (2017). DNA exonuclease Trex1 regulates radiotherapy-induced tumour immunogenicity. Nat. Commun. *8*, 15618.

iScience, Volume *23*

Supplemental Information

Intracellular C4BPA Levels Regulate NF-κB-Dependent Apoptosis

Monica M. Olcina, Ryan K. Kim, Nikolas G. Balanis, Caiyun Grace Li, Rie von Eyben, Thomas G. Graeber, Daniel Ricklin, Manuel Stucki, and Amato J. Giaccia

Supplemental Items

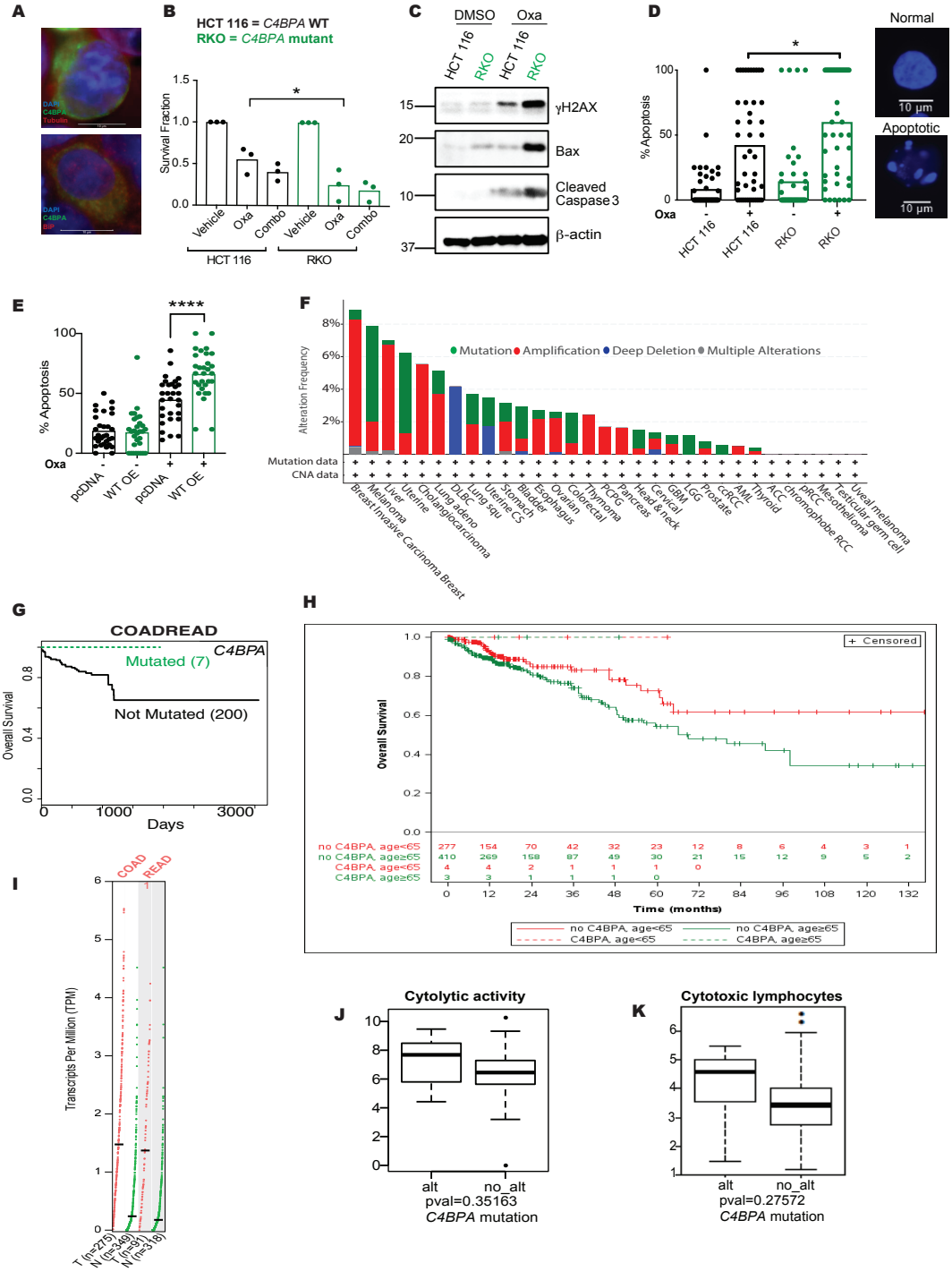

Figure S1: Intracellular C4BPA interacts with RelA, related to Figure 1. (A) HCT 116 *C4BPA*^{WT} were transfected with WT *C4BPA* and stained for C4BPA and Tubulin (top) or C4BPA and BiP (bottom). Representative images are shown. Scale bar (shown as white bar) = 10 μm. DAPI = blue. Differences in C4BPA staining reflect different levels of C4BPA following overexpression in different experiments. **(B)** Colony survival assay of RKO (colorectal cancer cells with endogenous *C4BPA* mutation) and HCT 116 (colorectal cancer cells without *C4BPA* mutation) treated with either DMSO, or oxaliplatin (40 μM, 1 hour) either alone or in combination with 5-FU (0.1 μg/ml, 1 hour). Individual dots represent values for each independent experiment (with three technical replicates per experiment), n = 3. Statistical significance was evaluated by two-way ANOVA, * = $p < 0.05$. **(C)** RKO (colorectal cancer cells with endogenous *C4BPA* mutation) and HCT 116 (colorectal cancer cells without *C4BPA* mutation) were treated with oxaliplatin 40 μM, 24 hours). Western blotting was carried out with the antibodies indicated. β-Actin was used as the loading control. n=3. **(D)** The graph represents the number of apoptotic/non-apoptotic cells expressed as a % of the whole population. HCT 116 and RKO cells treated with oxaliplatin (40 μM, 24 hours). Individual dots represent values for single fields of view in each individual independent experiment. n = 3. Statistical significance was evaluated by evaluated by two-way ANOVA, * = $p < 0.05$. A representative image of a normal (top) and apoptotic cell (bottom) is also shown to the left of the graph. **(E)** The graph represents the number of apoptotic/non-apoptotic cells expressed as a % of the whole population. HCT 116 cells were transfected with WT *C4BPA* (labeled WT OE) or empty vector (pcDNA 3.1). Cells were treated with oxaliplatin (40 μM, 24 hours). Individual dots represent values for single fields of view in each individual independent experiment. n = 3. Statistical significance was evaluated by two-way ANOVA, **** = $p < 0.0001$. **(F)** Graph showing the alteration frequency of mutations, amplifications, deep deletions or multiple alterations across cancer types. Data downloaded from cbioportal.org. **(G)** KM curve for overall survival of COADREAD patients with mutations in *C4BPA* vs patients without mutation (p=0.07001). **(H)** KM curve showing survival probability when COADREAD patients with *C4BPA* mutations are grouped according to age (product-limit survival estimates with number of subjects at risk). **(I)** *C4BPA* mRNA expression in tumor (T) and normal tissue (N) of patients with colon (COAD) or rectal (READ) cancer is shown. Log scale used = $Log_2(TPM+1)$. Each dot represents sample expression. Differential gene expression assessed by ANOVA. ILog_2FCI Cutoff = 1, q-value=0.01. **(J)** Immune infiltration signature associated with cytolytic activity was assessed in patients with and without *C4BPA* mutations in COADREAD patients. **(K)** Immune infiltration signature associated with cytotoxic lymphocytes was assessed in patients with and without *C4BPA* mutations in COADREAD patients. In boxplots, the box is drawn from the 25th (Q1) to the 75th (Q3) percentile. The horizontal line represents the 50th percentile or median. Whiskers extend to the maximum or minimum data values. If there are outliers (values extending beyond 1.5 x IQR), the whiskers extend to 1.5 x the IQR. IQR = Q3-Q1.

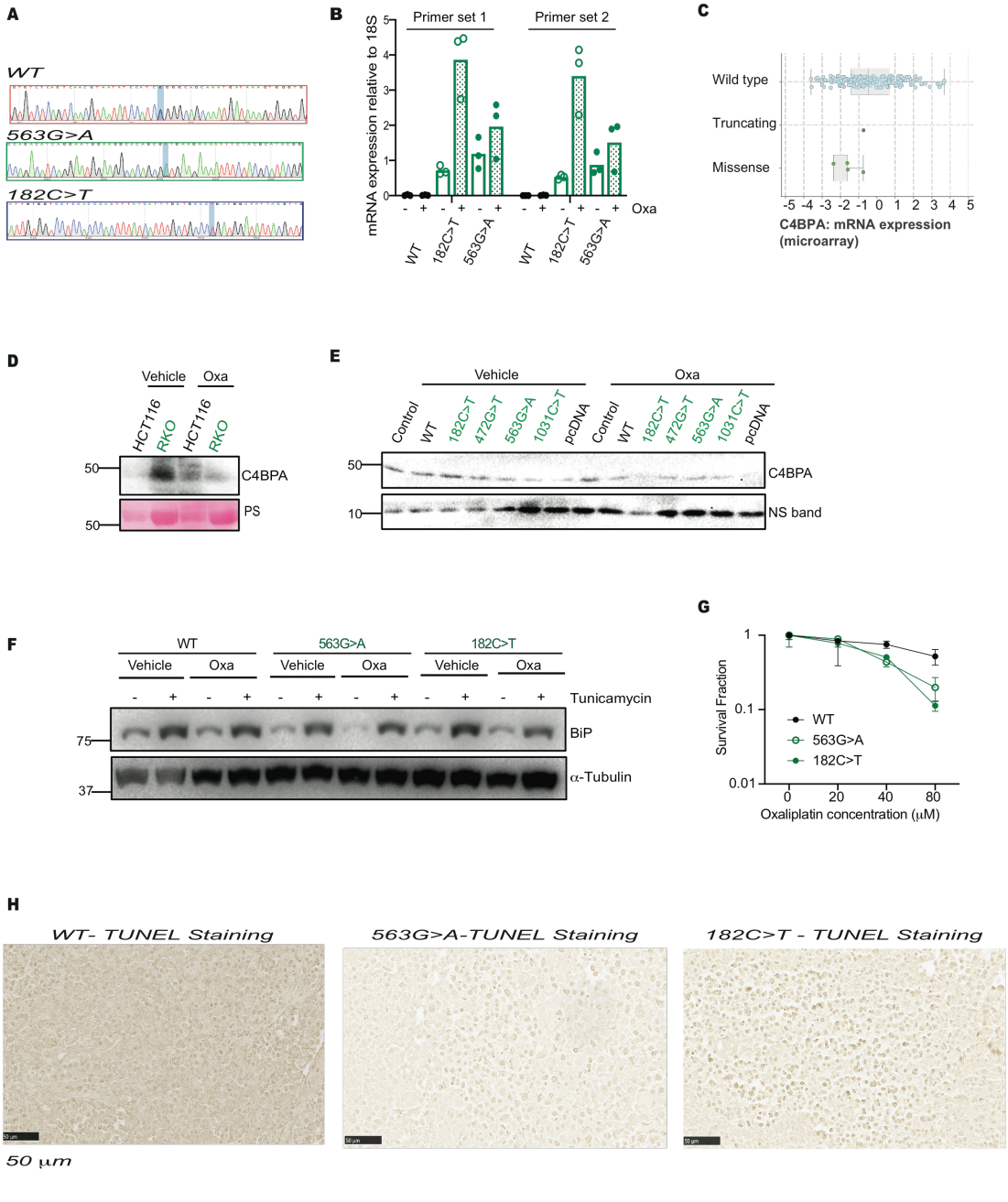
A
WT
563G>A
182C>T
B
Primer set 1
Primer set 2
mRNA expression relative to 18S
Oxa
WT
182C>T
563G>A
C
Wild type
Truncating
Missense
C4BPA: mRNA expression (microarray)
D
Vehicle
Oxa
HCT116
RKO
C4BPA
PS
E
Vehicle
Oxa
Control
pcDNA
C4BPA
NS band
F
WT
563G>A
182C>T
Tunicamycin
BiP
α-Tubulin
G
Survival Fraction
WT
563G>A
182C>T
Oxaliplatin concentration (μM)
H
WT- TUNEL Staining
563G>A-TUNEL Staining
182C>T - TUNEL Staining
50 μm

Figure S2: Patient-specific *C4BPA* mutants harbor increased intracellular C4BPA expression and apoptotic signaling in response to oxaliplatin, related to Figure 2. **(A)** HCT 116 cells with one of two specific *C4BPA* point mutations (563G>A or 182C>T, denoted HCT 116 *C4BPA*$^{563G>A}$ or HCT 116 *C4BPA*$^{182C>T}$ respectively) were generated by CRISPR/Cas9 technology. HCT 116 *C4BPA*^{WT} denotes HCT 116 cells that were targeted with a control vector so that no *C4BPA* mutation was introduced. Sequencing chromatograms are shown confirming the point mutations. Red chromatogram = HCT 116 *C4BPA*^{WT}, green chromatogram = HCT 116 *C4BPA*$^{563G>A}$ and blue chromatogram = HCT 116 *C4BPA*$^{182C>T}$. **(B)** mRNA expression of C4BPA/18S is shown. qPCR was carried out following treatment of HCT 116 *C4BPA*^{WT}, HCT 116 *C4BPA*$^{563G>A}$ or HCT 116 *C4BPA*$^{182C>T}$ with oxaliplatin (40 μM, 24 h), n=3. Individual dot represent average mRNA expression from each of 3 independent experiments. Data with 2 different C4BPA primers is shown. **(C)** C4BPA mRNA expression in patients with or without *C4BPA* mutations is shown. Data downloaded from cbioportal.org. In boxplots, the box is drawn from the 25th (Q1) to the 75th (Q3) percentile. The horizontal line represents the median. Whiskers extend to the maximum or minimum data values. If there are outliers (values extending beyond 1.5 x IQR), the whiskers extend to 1.5 x the IQR. IQR = Q3-Q1. **(D)** RKO and HCT 116 were treated with oxaliplatin (40 μM, 24 h) and conditioned media was collected. Western blotting was carried out with the antibodies indicated. Ponceau Staining (PS) was used as the loading control. n=3. **(E)** HCT 116 cells where C4BPA had been depleted by CRISPR/Cas9 technology were transfected with *C4BPA* mutant constructs, each representing a mutation found in cancer patients from the TCGA data set. Wild type (WT) *C4BPA* and empty pcDNA3.1 constructs were also transfected as controls. Cells were treated with oxaliplatin (40 μM, 24 hours) and conditioned media was collected. Western blotting was carried out with the antibodies indicated. Non-specific (NS) band was used as the loading control. n=3. **(F)** HCT 116 *C4BPA*^{WT}, HCT 116 *C4BPA*$^{563G>A}$ or HCT 116 *C4BPA*$^{182C>T}$ were treated with oxaliplatin (40 μM, 24 h). Western blotting was carried out with the antibodies indicated. α-Tubulin was used as the loading control. n=3. **(G)** Colony survival assay carried out following treatment of HCT 116 *C4BPA*^{WT}, HCT 116 *C4BPA*$^{563G>A}$ or HCT 116 *C4BPA*$^{182C>T}$ cells with different oxaliplatin doses (for 1 h). Individual dots represent technical replicates for an individual experiment. Error bars indicate standard deviation. (**H)** TUNEL staining was performed in tumors grown from HCT 116 *C4BPA*^{WT}, HCT 116 *C4BPA*$^{563G>A}$ or HCT 116 *C4BPA*$^{182C>T}$ cells and treated with oxaliplatin as in **(2E)**. Representative images for HCT 116 *C4BPA*^{WT}, HCT 116 *C4BPA*$^{563G>A}$ or HCT 116 *C4BPA*$^{182C>T}$ stained xenograft sections are shown.

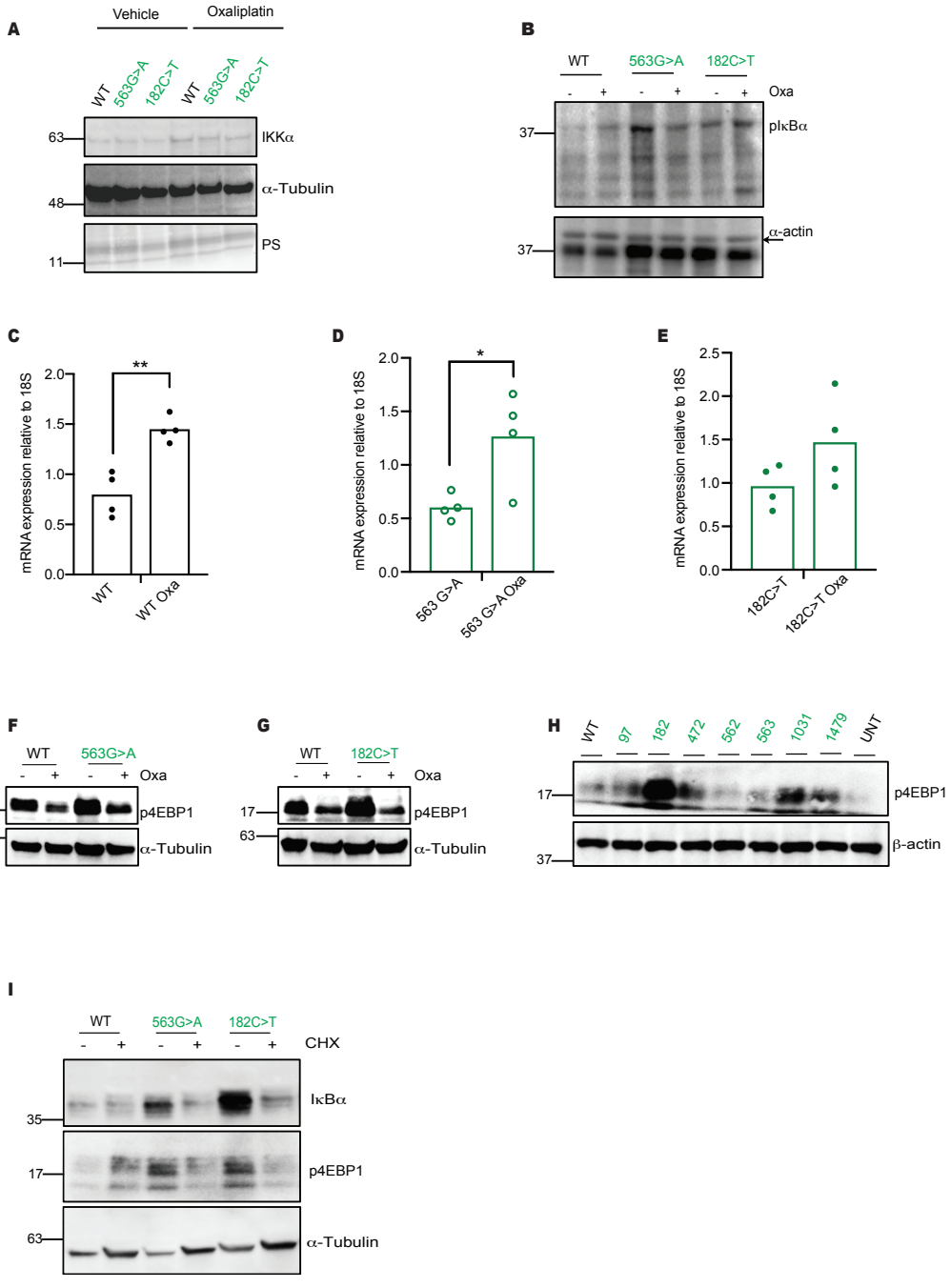
A
Vehicle
Oxaliplatin
WT
563G>A
182C>T
WT
563G>A
182C>T
63
IKKα
α-Tubulin
48
PS
11
B
WT
563G>A
182C>T
- + - + - +
Oxa
37
pIκBα
α-actin
37
C
mRNA expression relative to 18S
2.0
1.5
1.0
0.5
0.0
**
WT
WT Oxa
D
mRNA expression relative to 18S
2.0
1.5
1.0
0.5
0.0
*
563 G>A
563 G>A Oxa
E
mRNA expression relative to 18S
2.5
2.0
1.5
1.0
0.5
0.0
182C>T
182C>T Oxa
F
WT
563G>A
- + - +
Oxa
17
p4EBP1
63
α-Tubulin
G
WT
182C>T
- + - +
Oxa
17
p4EBP1
63
α-Tubulin
H
WT
97
182
472
562
563
1031
1479
UNT
17
p4EBP1
37
β-actin
I
WT
563G>A
182C>T
- + - + - +
CHX
35
IκBα
17
p4EBP1
63
α-Tubulin

Figure S3: Increased IκBα expression in *C4BPA* mutant cell lines is associated with increased translation markers, related to Figure 3. (A) HCT 116 *C4BPA*^{WT}, HCT 116 *C4BPA*$^{563G>A}$ or HCT 116 *C4BPA*$^{182C>T}$ were treated with oxaliplatin (40 μM, 24 h) Western blotting was carried out with the antibodies indicated. α-Tubulin was used as the loading control. PS = ponceau staining n=2. **(B)** HCT 116 *C4BPA*^{WT}, HCT 116 *C4BPA*$^{563G>A}$ or HCT 116 *C4BPA*$^{182C>T}$ were treated with oxaliplatin (Oxa, 40 μM, 24 h) Western blotting was carried out with the antibodies indicated. β-Actin was used as the loading control. n=2. **(C)** mRNA expression of IκBα/18S is shown. qPCR was carried out following treatment of HCT 116 *C4BPA*^{WT} cells with oxaliplatin (40 μM, 24 h), n=4. Individual dot represent average mRNA expression from each of 4 independent experiments. **(D)** mRNA expression of IκBα/18S is shown. qPCR was carried out following treatment of HCT 116 *C4BPA*$^{563G>A}$ cells with oxaliplatin (40 μM, 24 h), n=4. Individual dot represent average mRNA expression from each of 4 independent experiments. **(E)** mRNA expression of IκBα/18S is shown. qPCR was carried out following treatment of HCT 116 *C4BPA*$^{182C>T}$ cells with oxaliplatin (40 μM, 24 h), n=4. Individual dot represent average mRNA expression from each of 4 independent experiments. **(F)** HCT 116 *C4BPA*^{WT} or HCT 116 *C4BPA*$^{563G>A}$ were treated with oxaliplatin (Oxa, 40 μM, 24 h). Western blotting was carried out with the antibodies indicated. α-Tubulin was used as the loading control. n=2. **(G)** HCT 116 *C4BPA*^{WT} or HCT 116 *C4BPA*$^{182C>T}$ were treated with oxaliplatin (Oxa, 40 μM, 24 h). Western blotting was carried out with the antibodies indicated. α-Tubulin was used as the loading control. n=2. **(H)** HEK293T cells were transfected with different *C4BPA* mutants (corresponding to *C4BPA* mutations found in COADREAD patients), or WT *C4BPA*. UNT = Untransfected. Western blotting was carried out with the antibodies indicated. β-Actin was used as the loading control. n=2. **(I)** HCT 116 *C4BPA*^{WT}, HCT 116 *C4BPA*$^{563G>A}$ or HCT 116 *C4BPA*$^{182C>T}$ were treated with cycloheximide (CHX, 10 mg/ml, 24 h). Western blotting was carried out with the antibodies indicated. α-Tubulin was used as the loading control. n=3.

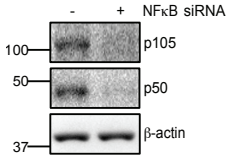

Figure S4: Altered NF-κB signaling regulates apoptosis in patient-specific *C4BPA* mutant backgrounds, related to Figure 4. HCT 116 *C4BPA*^{WT} cells were transfected with either scramble (Scr) or NF-κB1 siRNA. Western blotting was carried out with the antibodies indicated. β-Actin was used as the loading control. n=3.

Protein Change	Copy #	HGVSc
G188S	diploid	ENST00000367070.3:c.562G>A
L33I	gain	ENST00000367070.3:c.97C>A
P61L	gain	ENST00000367070.3:c.182C>T
T344M	diploid	ENST00000367070.3:c.1031C>T
E596*	diploid	ENST00000367070.3:c.1786G>T
D158Y	diploid	ENST00000367070.3:c.472G>T
R493S	diploid	ENST00000367070.3:c.1479G>T

Table S1, relating to Figure 1. Table summarizing the *C4BPA* mutations found in colorectal cancer patients from TCGA data sets. Data downloaded from cbioportal.org.

Term	PValue	Fold Enrichment	Bonferroni	Benjamini	FDR
GO:0042981	3.73E-08	8.07641791	2.87E-05	2.87E-05	5.70E-05
GO:0043067	4.13E-08	7.996847291	3.18E-05	1.59E-05	6.31E-05
GO:0010941	4.29E-08	7.967411043	3.31E-05	1.10E-05	6.56E-05
GO:0043066	1.87E-06	12.22870056	0.00143635	3.59E-04	0.00285101
GO:0043069	2.05E-06	12.0583844	0.00157689	3.16E-04	0.00313018
GO:0060548	2.09E-06	12.02488889	0.00160634	2.68E-04	0.00318868
GO:0010033	2.09E-06	7.505131761	0.00161054	2.30E-04	0.00319703
GO:0009725	2.37E-06	11.79553134	0.00182566	2.28E-04	0.00362443
GO:0007242	3.38E-06	5.169936306	0.0026007	2.89E-04	0.00516507
GO:0042127	4.32E-06	6.875730623	0.0033182	3.32E-04	0.00659237
GO:0009719	4.56E-06	10.68879012	0.00350299	3.19E-04	0.00696014
GO:0042325	1.14E-05	9.289613734	0.00877051	7.34E-04	0.01747151
GO:0019220	1.48E-05	8.925690722	0.0113615	8.79E-04	0.02266197
GO:0051174	1.48E-05	8.925690722	0.0113615	8.79E-04	0.02266197
GO:0006916	2.62E-05	15.7607767	0.01996373	0.00143937	0.03999064
GO:0042493	3.29E-05	15.03111111	0.02499962	0.0016864	0.05020449
GO:0009968	3.67E-05	14.69104072	0.02785446	0.00176405	0.05601767
GO:0014070	5.63E-05	22.36033058	0.04245696	0.00254878	0.08601634
GO:0010648	6.36E-05	13.0916129	0.04776105	0.00271516	0.09702394
GO:0010604	7.42E-05	5.682707118	0.05551888	0.00300178	0.11323251
GO:0001666	8.39E-05	20.19104478	0.06253293	0.00322348	0.12799981
GO:0070482	1.02E-04	19.18865248	0.07566942	0.00373992	0.15595092
GO:0044087	1.05E-04	19.05352113	0.0776868	0.00366918	0.16027785
GO:0006468	1.14E-04	6.490194903	0.08385787	0.00380075	0.17357153

Table S2. Relating to Figure 1. Table summarizing data from Gene Ontology analysis of proteins differentially expressed in COADREAD patients with *C4BPA* mutations compared to patients without *C4BPA* mutations (From TCGA RPPA analysis data).

Transparent Methods

"Further information and requests for resources and reagents should be directed to and will be fulfilled by the Lead Contact, Monica Olcina (monica.olcinadelmolino@uzh.ch).

KEY RESOURCES TABLE

REAGENT or RESOURCE	SOURCE	IDENTIFIER
Antibodies		
C4BPA	Thermo-Fisher Scientific	Cat# PA5-25861 RRID:AB_2543361
β-actin	Sigma-Aldrich	Cat# A5441 RRID:AB_476744
γH2AX	Upstate Millipore	Cat# 07-164 RRID: AB_310406
Cleaved Caspase-3 (Asp175)	Cell Signaling Technology	Cat# 9661 RRID: AB_2341188
Bax	Cell Signaling Technology	Cat# 2774 RRID: AB_490806
RelA	Cell Signaling Technology	Cat# 3034 and 8242 RRID:AB_330561 and RRID:AB_10859369
RelA	Bethyl	Cat# A301-824A-M RRID: AB_2780149
IκBα	Novus	Cat# NB100-56507, RRID:AB_838388
IκBα (L35A5)	Cell Signaling Technology	Cat# 4814 ¡
p105/p50 NFκB1 (D7H5M)	Cell Signaling Technology	Cat# 12540 RRID:AB_2687614
α-Tubulin	Fitzgerald	Cat# I0R-T130A RRID:AB_1279269
α-Tubulin DM1A	Sigma-Aldrich	Cat# T6199 RRID:AB_477583
hFAB™ Rhodamine Anti-Tubulin	Bio-Rad	Cat#12004166
Lamin A/C	Cell Signaling Technology	Cat# 2032 RRID:AB_2136278
Phospho-IκBα (Ser32)	Cell Signaling Technology	Cat# 2859
IKKα	Cell Signaling Technology	Cat# 2682 RRID:AB_331626
Phospho-4EBP1 Thr37/46	Cell Signaling Technology	Cat# 2855P

GRP78/HSPA5/BiP	R&D Systems	Cat # MAB4846 RRID:AB_2233235
Alexa-Fluor A459 anti-rabbit IgG	Invitrogen	Cat# A-21207 RRID:AB_141637
Alexa-Fluor A488 anti-mouse IgG	Invitrogen	Cat# A-21202 RRID:AB_141637
Alexa-Fluor A488 anti-rabbit IgG	Invitrogen	Cat# A-11008 RRID:AB_143165
Alexa-Fluor A647 anti-mouse IgG	Invitrogen	Cat# A-21235 RRID:AB_2535804
Mouse anti-Rabbit IgG	Jackson ImmunoResearch Labs	Cat# 211-032-171 RRID:AB_2339149
Goat anti-mouse IgG	Jackson ImmunoResearch Labs	Cat# 115-035-174 RRID:AB_2338512
Critical Commercial Assays		
ApopTag® Peroxidase In Situ Apoptosis Detection Kit	Millipore	Cat# 7100
NF-κB assay	BPS Biosciences	Cat# 60614
QuickChange® Site-directed mutagenesis kit	Agilent	Cat# 200521
Fractionation Kit	Cell Signaling Technology	Cat #9038
Raw and analyzed data	This paper	Supplemental Tables
Experimental Models: Cell Lines		
HCT 116	ATCC®	Cat# CCL-247™ RRID:CVCL_0291
RKO	ATCC®	Cat# CRL-2577 RRID:CVCL_0504
HEK293T	ATCC®	Cat# CRL-3216 RRID:CVCL_0063
HCT 116 *C4BPA*^{WT} HCT 116 *C4BPA*$^{182C>T}$ HCT 116 *C4BPA*$^{563G>A}$	Biocytogen	Cell lines generated for this manuscript
Oligonucleotides		
ON-TARGETplus Non-targeting Pool	Dharmacon	D-001810
SMARTpool: ON-TARGETplus RelA siRNA	Dharmacon	L-003533
SMARTpool: ON-TARGETplus NFKBIA siRNA	Dharmacon	J-004765
SMARTpool: ON- NFκB1 TARGETplus siRNA	Dharmacon	L-003520
Recombinant DNA		
pcDNA 3.1	-	Cat# V790-20

C4BPA	Origene	Cat# SC119723
PMX459 (gRNA CACCGACAAACGATGCAG ACACCC)	Addgene (Zhang lab)	-
Software and Algorithms		
DESeq2	(Love et al., 2014)	RRID: SCR_015687
GSEA		RRID:SCR_003199
RPPA		RRID: SCR_016649
MCP-counter	(Becht et al., 2016a)(Becht et al., 2016b)	http://cit.ligue-cancer.net/language/en/mcp-counter/
SSGSEA	Hanzelmann S,et al	https://bioconductor.org/packages/release/bioc/html/GSVA.html
GraphPad Prism version 8.0c	GraphPad Software	N/A

Cell lines and treatments. RKO and HCT 116 (human colorectal cancer), cells originally purchased from ATCC® were a kind gift Ester Hammond (Oxford, UK). HEK293T cells were purchased from ATCC®. Cells were grown in DMEM with 10% FBS, in a standard humidified incubator at 37°C and 5% CO_2. All cell lines were routinely mycoplasma tested and found to be negative. Oxaliplatin (Oxa) was used at a range of concentrations for either 1 or 24 hours as stated in figure legends. 5-fluorouracil (5-FU) was used at a concentration of 0.1 μg/ml for either 1 or 24 hours as stated in the figure legends. ACHP (Tocris) was used at a concentration of 25 μM as previously described (Sanda et al., 2005). Cycloheximide (CHX) (Sigma-Aldrich) was used at a concentration of 10 μg/ml. Tunicamycin (Sigma-Aldrich) was used at a concentration of 1 μg/ml.

CRISPR/Cas9 mediated depletion of C4BPA was performed as previously

described (Ran et al., 2013). sgRNA sequence (CACCGACAAACGATGCAGACACCC) was cloned into PMX459 vector containing Cas9. This plasmid was transfected into HCT 116. Clones were isolated following puromycin selection.

CRISPR/Cas9 mediated generation of stable *C4BPA* point mutation cell lines was carried out using the CRISPR/Cas9 based EGE system (Biocytogen). In brief, sgRNA and targeting vector were electroporated into HCT 116 cells. sgRNAs were designed to target c.C182T, p61L (resulting cell line named HCT 116 *C4BPA*$^{182C>T}$) and cG563A, pG188D. (HCT 116 *C4BPA*$^{563G>A}$). sgRNAs were designed for high activity and low off-target effects. Two separate clones for each mutation were tested in functional assays. Colonies were picked following puromycin selection and screened by PCR. Following clonal growth of cells in semisolid media, resistant clones were picked and expanded for further analysis including validation by sequencing (Figure S2). Clones that were transfected but where *C4BPA* was not mutated are designated HCT 116 *C4BPA* ^{WT} and were used as controls.

DNA Transfections. *C4BPA* point mutants were generated with the use of the QuickChange® Site-directed mutagenesis kit (Agilent). Point mutations corresponding to coding missense mutations found in colorectal cancer TCGA patients were generated and transfected with the use of Lipofectamine 2000 (Invitrogen) into HCT 116 where C4BPA had been depleted by CRISPR/Cas9.

siRNA transfection. RelA, IκBα, NFκB1 siRNA pool (Dharmacon) or non-targeting RNAi negative control (Dharmacon) were transfected into HCT 116^{WT}, HCT $116^{563G>A}$ or HCT $116^{182C>T}$ cells using RNAi Max (Invitrogen) at a final concentration of 50 nM; according to the manufacturers' instructions. Cells were harvested 72 hours post- transfection.

NF-κB reporter assay. NF-κB reporter kit was used (BPS Biosciences #60614) according to manufacturer's instructions. NF-κB luciferase reporter vector constitutively expressing a *Renilla* luciferase vector was transfected into HCT 116 *C4BPA* ^{WT}, HCT 116 *C4BPA* $^{563G>A}$ or HCT 116 *C4BPA* $^{182C>T}$ cells with Lipofectamine 3000 (Invitrogen). Negative control reporter consisting of a non-inducible luciferase vector also constitutively expressing a *Renilla* luciferase vector was also transfected. 48 hours post-transfection cells were treated with 40 μM oxaliplatin (Sigma-Aldrich) or vehicle (H_2O). 6 hours of TNFα treatment (Sigma-Aldrich) was used as positive control for NF-κB induction. ACHP (Tocris) was used at a concentration of 25 μM as a negative control for NF-κB activity. Luciferase activity was measured using the Dual-Reporter® Assay System (Promega). Luciferase reading was divided by the *Renilla* reading to calculate the NF-κB activity. Background reading corresponds to the reading of the wells transfected with negative control vector. NF-κB activity-background is shown. Three independent experiments were carried out.

Immunoblotting. Sample preparation and immunoblotting was carried out as stated in Mendeley Data: https://data.mendeley.com/datasets/sks63zhwby/1. Briefly, cells were lysed in UTB (9 M urea, 75 mM Tris-HCl pH 7.5 and 0.15 M β-mercaptoethanol) and sonicated briefly. Antibodies used were: C4BPA (Thermo-Fisher Scientific), β-actin (Santa Cruz), γH2AX (Upstate), α-tubulin (Fitzgerald and Sigma-Aldrich), hFAB™ Rhodamine Anti-Tubulin (Bio-Rad), total IκBα (Cell Signaling Technology and Novus). RelA/p65 (Cell Signaling Technology and Bethyl) p105/p50 NFκB1, Lamin A/C, Bax, Cleaved Caspase 3, phospho-4E-BP1 Thr37/46, IKKα , Phospho-IκBα (Ser32) (Cell Signaling Technology) and GRP78/HSPA5/BiP (R&D systems). The BioRad Chemidoc XRS system was used. In each case experiments were carried out in triplicate and a representative blot is shown unless otherwise stated.

Immunoprecipitation. Immunoprecipitation was carried out as in (Li et al., 2019). Whole cell extracts were incubated overnight with antibodies at 4^{o}C while rotating. The following day, extracts were incubated for 3 hours at 4^{o}C with protein G Dynabeads (Thermo Fisher Scientific) while rotating. Beads were washed three times with ice-cold wash buffer (50 mM Tris-HCl, pH 7.5, 150 mM NaCl, 1 mM EDTA, 0.05% NP-40) following incubation. Elution of proteins was carried out with IgG elution buffer (Thermo Fisher Scientific) at room temperature for 10 minutes on gentle vortex. The final elution was collected and neutralized using 1/10 volumes of 1 M Tris-HCl, pH 9.0. RelA immunoprecipitation was carried out with RelA antibody (Bethyl). Secondary antibody mouse-anti-rabbit

and goat anti-mouse antibodies were used (as stated in the Key Resource Table).

Subcellular fractionation. The Cell Signaling Technology fractionation kit (Cell Signaling Technology, cat# 9038) was used according to manufacturer's instructions. Cells were harvested into 0.5 ml ice-cold PBS and counted using Trypan Blue and Countess™ II automated cell counter. For every 5 x 10^6 cells, 100 μl of suspension was aliquoted as whole cell lysate (WCL). The remaining sample was centrifuged for 5 minutes at 500 x g at 4°C and the pellet was resuspended in 500 μl of "cytoplasminc isolation" buffer. Following a 5 second vortex and 5 minute incubation on ice the sample was centrifuged for 5 minutes at 500 x g and the supernatant was saved as the cytoplasmic fraction. The remaining pellet was resuspended in 500 μl of "membrane and organelle isolation" buffer and vortexed for 15 seconds and incubated on ice for 5 minutes followed by centrifugation for 5 minutes at 8000 x g. The remaining supernatant was collected as the membrane/organelle fraction. The pellet was resuspended in 250 μl of "cytoskeleton/nucleus isolation" buffer and sonicated for 5 seconds on medium power using a Bioruptor® (Diagenode). Western blotting was then carried out as described above. An adapted version of the REAP fractionation method was also used (Suzuki et al., 2010). Cells were harvested in 1 ml ice-cold PBS followed by centrifugation at top speed for 10 seconds at 4°C. Pellets were resuspended in 900 μl of 0.1% NP-40 in PBS. 300 μl of this suspension was saved as WCL. The remaining sample was centrifuged at 13000 x g, 4 °C for 10

seconds and 300 μl of supernatant was aliquoted as the cytoplasmic fraction. The remaining pellet was resuspended in 0.1% NP-40 in PBS and centrifuged at 13000 x g, 4 ^{o}C for 10 seconds. The remaining pellet was resuspended in 100-180 μl (depending on size) of 0.1% NP-40. Protein was quantified (using Pierce^{TM} BCA protein assay kit, ThermoFisher Scientific, cat #23225) and western blotting was carried out as stated above.

Immunofluorescence. Staining was carried out as previously described and as stated in Mendeley Data: https://data.mendeley.com/datasets/sks63zhwby/1 using C4BPA antibody (Thermo-Fisher Scientific), hFAB^{TM} Rhodamine anti-tubulin (BioRad) or BiP (Novus) (Olcina et al., 2013). Cells were visualized using a DSM6000, DMi8 or DMI6000 (Leica) microscope. In each case experiments were carried out at least in triplicate.

Apoptosis assays. Apoptosis counts were performed as previously described by assessing morphology following DAPI staining (Olcina et al., 2015). Adherent and detached cells (in media) were collected and fixed in 4% PFA for 15 minutes at room temperature. PFA was removed and cells were washed in 1 ml PBS. 10 μl of fixed cells in PBS was placed in each slide and mixed with ProLong® Gold mounting medium with DAPI (Invitrogen/Life technologies). A coverslip was placed on top of the sample and slides were left to dry overnight. Slides were imaged using a DSM6000, DMi8 or DMI6000 (Leica) microscope with 40x or 60x oil objectives. The number of cells with fragmented DNA and the total number of

cells per field was counted (with typically at least 10 fields counted for every treatment).

TUNEL assay (Millipore) was used to stain 4 μm paraffin-embedded tumor sections. Stained slides were scanned with a NanoZoomer 2.0-RS Digital Slide Scanner (Hamamatsu). 15 randomly chosen fields of view (from at least 2 different tumors per condition) at 10x magnification were selected for analysis via ImageJ software (NIH). Images were first converted to 8-bit black and white, then the threshold was adjusted to 0-200 to eliminate background signal. The remaining particles larger than 10 square pixels were counted.

Clonogenic survival assay. Colonies (of at least 50 cells) were allowed to form for 10-14 days. Colonies were then stained with crystal violet and counted. Clonogenic survival was determined by dividing the number of counted colonies by the number of cells plated.

Xenograft study. HCT 116 *C4BPA* ^{WT}, HCT 116 *C4BPA* $^{563G>A}$ or HCT 116 *C4BPA* $^{182C>T}$ cells (1.5×10^6) were injected subcutaneously into 8-10 week old female Athymic nude mice (Charles Rivers) at a single dorsal site. Growing tumors (average, 60-90 mm^3) were treated with oxaliplatin (10 mg/kg) at day 0 and 3. Tumors were measured with the use of calipers and volumes calculated by the ellipsoid estimation method as previously described (Taniguchi et al., 2014). All procedures were performed in accordance with the National Institutes

of Health (NIH) guidelines for the use and care of live animals (approved by the Stanford University Institutional Animal Care and Use Committee).

qPCR. RNA was extracted using Trizol (Invitrogen/Life Technologies). iScript cDNA synthesis kit was used to reverse transcribe cDNA from total RNA according to manufacturer's instructions. Relative mRNA levels were calculated using the standard curve methodology. Primers used: 18S F: TAGAGGGACAAGTGGCGTTC, 18S R: CGGACATCTAAGGGCATCAC. C4BPA F1: TTCACACTGGTCAGCTCCAG, C4BPA R1: GGTTCTGTTCCCAGAGCAAG, C4BPA F2: GGTTCTGTTCCCAGAGCAAG, C4BPA R2: TGGGTACCAGGTTCTGTTCC, NFKBIAF: ACCTGGTGTCACTCCTGTTGA, NFKBIAR: CTGCTGCTGTATCCGGGTG

TCGA RNA-sequencing (RNA-seq) analysis. TCGA raw counts were acquired from the TCGA data portal using TCGA-Assembler. Counts were rounded then inputted into DESeq2 to perform differential expression analysis using default size factor normalization (Love et al., 2014). The Independent filtering and Cooks Cutoff flags were set to FALSE. Benjamini–Hochberg method was used for multiple hypothesis testing.

GSEA. Gene set enrichment analysis was performed on the output of DESeq2 as defined earlier using COADREAD expression data where groups were defined

by C4BPA mutational status. GSEA preranked was used with the signed log p-value output of DESeq2 as the ranking metric.

Clinical association analysis. For the association of mutations to survival, somatic mutations were only evaluated if they occurred in at least 3 samples. Pan-cancer level survival analysis was performed using a multivariable cox regression on mutational status controlling for type, age and gender (coxph in R). Wald test p-values are reported. Individual cancers were evaluated with a univariate model on mutational status.

RPPA data analysis. Significantly differentially expressed RPPA data was obtained using rowttests in the genefilter package from TCGA patients with *C4BPA* mutations compared to patients without mutations and was analyzed though DAVID Bioinformatics Resources (6.7) Functional annotation tool (using Ensemble gene ID) (accessed August 4 2016)[1,12]. Only expression changes with $p<0.05$ were included in the list. GOTERM_BP_FAT was used as the category.

Immune infiltration analysis. Samples with and without *C4BPA* mutations were compared for enrichment of immune infiltration signatures using RNAseq data. Single sample GSEA (ssGSEA) was performed with immune signatures derived from MCP-counter (Becht et al., 2016a)(Becht et al., 2016b). ssGSEA scores were compared between mutant and non mutant groups using a student's t-test to find significant differences in cytolytic activity and cytotoxic lymphocytes.

Differential tumor vs normal tissue expression data analysis. C4BPA mRNA expression data for tumor and normal tissue of patients with colon (COAD) or rectal (READ) cancer was accessed and downloaded through GEPIA (http://gepia.cancer-pku.cn)(July 2nd 2020). Matched TCGA normal and GTEx data is shown. Differential gene expression assessed by ANOVA. $|Log_2FC|$ Cutoff = 1, q-value=0.01.

References

Becht, E., De Reyniès, A., Giraldo, N.A., Pilati, C., Buttard, B., Lacroix, L., Selves, J., Sautès-Fridman, C., Laurent-Puig, P., and Fridman, W.H. (2016a). Immune and stromal classification of Colorectal cancer is associated with molecular subtypes and relevant for precision immunotherapy. Clin. Cancer Res. *22*, 4057–4066.

Becht, E., Giraldo, N.A., Lacroix, L., Buttard, B., Elarouci, N., Petitprez, F., Selves, J., Laurent-Puig, P., Sautès-Fridman, C., Fridman, W.H., et al. (2016b). Estimating the population abundance of tissue-infiltrating immune and stromal cell populations using gene expression. Genome Biol. *17*, 218.

Huang, D.W., Sherman, B.T., and Lempicki, R.A. (2008). Systematic and integrative analysis of large gene lists using DAVID bioinformatics resources. Nat. Protoc. *4*, 44–57.

Huang, D.W., Sherman, B.T., and Lempicki, R.A. (2009). Bioinformatics enrichment tools: Paths toward the comprehensive functional analysis of large gene lists. Nucleic Acids Res. *37*, 1–13.

LaGory, E.L., Wu, C., Taniguchi, C.M., Ding, C.K.C., Chi, J.T., von Eyben, R., Scott, D.A., Richardson, A.D., and Giaccia, A.J. (2015). Suppression of PGC-1α Is Critical for Reprogramming Oxidative Metabolism in Renal Cell Carcinoma. Cell Rep. *12*, 116–127.

Li, C.G., Mahon, C., Sweeney, N.M., Verschueren, E., Kantamani, V., Li, D., Hennigs, J.K., Marciano, D.P., Diebold, I., Abu-Halawa, O., et al. (2019). PPARγ Interaction with UBR5/ATMIN Promotes DNA Repair to Maintain Endothelial Homeostasis. Cell Rep.

Love, M.I., Huber, W., and Anders, S. (2014). Moderated estimation of fold change and dispersion for RNA-seq data with DESeq2. Genome Biol. *15*, 550.

Olcina, M.M., Foskolou, I.P., Anbalagan, S., Senra, J.M., Pires, I.M., Jiang, Y., Ryan, A.J., and Hammond, E.M. (2013). Replication stress and chromatin context link ATM activation to a role in DNA replication. Mol. Cell *52*, 758–766.

Olcina, M.M., Leszczynska, K.B., Senra, J.M., Isa, N.F., Harada, H., and Hammond, E.M. (2015). H3K9me3 facilitates hypoxia-induced p53-dependent apoptosis through repression of APAK. Oncogene.

Ran, F.A., Hsu, P.D., Wright, J., Agarwala, V., Scott, D.A., and Zhang, F. (2013). Genome engineering using the CRISPR-Cas9 system. Nat. Protoc. *8*, 2281–2308.

Sanda, T., Iida, S., Ogura, H., Asamitsu, K., Murata, T., Bacon, K.B., Ueda, R., and Okamoto, T. (2005). Growth inhibition of multiple myeloma cells by a novel IkappaB kinase inhibitor. Clin. Cancer Res. *11*, 1974–1982.

Suzuki, K., Bose, P., Leong-Quong, R.Y., Fujita, D.J., and Riabowol, K. (2010). REAP: A two minute cell fractionation method. BMC Res. Notes.

Taniguchi, C.M., Miao, Y.R., Diep, A.N., Wu, C., Rankin, E.B., Atwood, T.F., Xing, L., and Giaccia, A.J. (2014). PHD inhibition mitigates and protects against radiation-induced gastrointestinal toxicity via HIF2. Sci. Transl. Med. *6*, 236ra64.